

THE PHYSICAL CHEMISTRY OF MATERIALS



ENERGY AND
ENVIRONMENTAL APPLICATIONS

ROLANDO M.A. ROQUE-MALHERBE



CRC Press
Taylor & Francis Group

**THE PHYSICAL
CHEMISTRY OF
MATERIALS**

**ENERGY AND
ENVIRONMENTAL APPLICATIONS**

THE PHYSICAL CHEMISTRY OF MATERIALS

ENERGY AND
ENVIRONMENTAL APPLICATIONS

ROLANDO M.A. ROQUE-MALHERBE



CRC Press

Taylor & Francis Group

Boca Raton London New York

CRC Press is an imprint of the
Taylor & Francis Group, an **informa** business

CRC Press
Taylor & Francis Group
6000 Broken Sound Parkway NW, Suite 300
Boca Raton, FL 33487-2742

© 2010 by Taylor and Francis Group, LLC
CRC Press is an imprint of Taylor & Francis Group, an Informa business

No claim to original U.S. Government works

Printed in the United States of America on acid-free paper
10 9 8 7 6 5 4 3 2 1

International Standard Book Number: 978-1-4200-8272-2 (Hardback)

This book contains information obtained from authentic and highly regarded sources. Reasonable efforts have been made to publish reliable data and information, but the author and publisher cannot assume responsibility for the validity of all materials or the consequences of their use. The authors and publishers have attempted to trace the copyright holders of all material reproduced in this publication and apologize to copyright holders if permission to publish in this form has not been obtained. If any copyright material has not been acknowledged please write and let us know so we may rectify in any future reprint.

Except as permitted under U.S. Copyright Law, no part of this book may be reprinted, reproduced, transmitted, or utilized in any form by any electronic, mechanical, or other means, now known or hereafter invented, including photocopying, microfilming, and recording, or in any information storage or retrieval system, without written permission from the publishers.

For permission to photocopy or use material electronically from this work, please access www.copyright.com (<http://www.copyright.com/>) or contact the Copyright Clearance Center, Inc. (CCC), 222 Rosewood Drive, Danvers, MA 01923, 978-750-8400. CCC is a not-for-profit organization that provides licenses and registration for a variety of users. For organizations that have been granted a photocopy license by the CCC, a separate system of payment has been arranged.

Trademark Notice: Product or corporate names may be trademarks or registered trademarks, and are used only for identification and explanation without intent to infringe.

Library of Congress Cataloging-in-Publication Data

Roque-Malherbe, Rolando M. A.

The physical chemistry of materials : energy and environmental applications / Rolando M.A.

Roque-Malherbe.

p. cm.

Includes bibliographical references and index.

ISBN 978-1-4200-8272-2 (hardcover : alk. paper)

1. Materials science. 2. Chemistry, Physical and theoretical. I. Title.

TA403.R567 2010

620.1'1--dc22

2009034795

Visit the Taylor & Francis Web site at
<http://www.taylorandfrancis.com>

and the CRC Press Web site at
<http://www.crcpress.com>

*To the loving memory of my mother, Silvia Malherbe;
my father, Rolando Roque;
my grandmothers, Maria Fernandez and Isidra Peña;
my grandfathers, Herminio Roque and Diego Malherbe;
and my favorite pets, Zeolita and Trosia*

Contents

Preface.....	xix
Author	xxi
Chapter 1 Materials Physics.....	1
1.1 Introduction	1
1.2 Crystallography	1
1.2.1 Crystalline Structure	1
1.2.2 Crystallographic Directions and Planes	5
1.2.3 Octahedral and Tetrahedral Sites in the FCC Lattice	5
1.2.4 Reciprocal Lattice	6
1.3 Bloch Theorem	7
1.4 Lattice Vibrations	10
1.4.1 Phonons	10
1.4.2 Bose–Einstein Distribution	13
1.4.3 Heat Capacity of Solids	14
1.5 Electrons in Crystalline Solid Materials	17
1.5.1 Electron Gas	17
1.5.2 Fermi–Dirac Distribution.....	19
1.5.3 Density of States for the Electron Gas	21
1.5.4 Energy Band Model.....	24
1.5.5 Molecular Orbital Approach for the Formation of Energy Bands	26
1.6 X-Ray Diffraction.....	30
1.6.1 General Introduction	30
1.6.2 X-Ray Scattering	31
1.6.3 Diffraction Conditions	33
1.6.4 Powder Diffraction Method	35
1.6.5 Other Factors Affecting the Scattering Intensity of a Powdered Sample	36
1.6.5.1 Multiplicity Factor	36
1.6.5.2 Lorentz Factor.....	37
1.6.5.3 Absorption Factor	37
1.6.5.4 Temperature Factor.....	38
1.6.6 Intensity of a Diffraction Peak	38
1.7 Dielectric Phenomena in Materials	39
1.7.1 Introduction	39
1.7.1.1 Electronic Polarization	39
1.7.1.2 Ionic Polarization.....	39
1.7.1.3 Dipolar (or Orientation) Polarization.....	40
1.7.1.4 Hopping of Charge Carriers’ Polarization.....	40
1.7.1.5 Interfacial Polarization	40
1.7.2 Susceptibility and Dielectric Constant.....	40
1.7.3 Complex Permittivity	41
1.7.4 Dielectric Relaxation	42
1.7.5 Debye Relaxation Model for the Dipolar Mechanism	44

1.7.6	Model to Describe Dielectric Relaxation for a Charge Hopping Process.....	46
1.8	Nuclear Magnetic Resonance	52
1.8.1	Introduction	52
1.8.2	Nuclear Zeeman Effect	53
1.8.3	Magnetization and Time Evolution of the Magnetization.....	54
1.8.4	Nuclear Magnetic Resonance Experiment.....	56
1.8.5	Spin-Lattice Relaxation Time (T_1), Spin-Spin Relaxation Time (T_2), and the Bloch Equations.....	56
1.9	Mössbauer Effect.....	58
1.9.1	Introduction	58
1.9.2	Mössbauer Effect.....	58
	References	60

Chapter 2	Structure of Adsorbents, Ion Exchangers, Ion Conductors, Catalysts, and Permeable Materials	63
2.1	Introduction	63
2.2	Transition Metal Catalysts.....	63
2.2.1	Metallic Catalysts' Performance.....	63
2.2.2	Band Structure of Transition Metals	64
2.2.3	Body-Centered Cubic Iron as a Catalyst.....	64
2.2.4	Face-Centered Cubic Platinum as a Catalyst	65
2.2.5	Hexagonal Close-Packed Cobalt as a Catalyst.....	66
2.2.6	Balandin Volcano Plot.....	66
2.3	Nonmetallic Catalysts	67
2.3.1	Simple Oxides	67
2.3.2	Rock-Salt-Structure Catalysts	68
2.3.3	Rutile-Type Catalyst	68
2.3.4	Corundum-Type Catalysts.....	69
2.3.5	Wurtzite-Type Catalysts	71
2.3.6	Fluorite-Type Catalysts	71
2.3.7	Spinel-Type Catalysts	71
2.3.8	Zinc Blende-Type Structure.....	72
2.4	Permeable Materials	73
2.4.1	Introduction	73
2.4.2	Palladium: A Hydrogen Permeable Material	73
2.4.3	Yttrium Oxide (Y_2O_3)-Stabilized Zirconium Oxide (ZrO_2)	74
2.4.4	Hydrogen-Permeable Perovskites.....	74
2.4.5	Silver Iodide: A Fast Ion Conductor	75
2.5	Crystalline and Ordered Nanoporous Adsorbents and Catalysts.....	76
2.5.1	Zeolite Adsorbents	76
2.5.2	Mesoporous Molecular Sieve Adsorbents.....	78
2.5.3	Zeolite Catalysts.....	79
2.5.4	Pillared Clay Catalysts	79
2.6	Ion-Exchange Crystalline Materials.....	80
2.6.1	Zeolites	80
2.6.2	Hydrotalcites	81

2.6.3	Titanates	82
2.6.3.1	Alkali Metal Titanates.....	82
2.6.3.2	Titanium Silicates	82
2.6.4	Zirconium Phosphates	83
2.7	Amorphous Silica Adsorbents and Catalytic Supports	84
2.7.1	Amorphous Silica.....	84
2.7.2	Amorphous Silica as Adsorbents and Catalytic Supports	86
2.8	Active Carbon and Other Carbon Forms as Adsorbents and Catalytic Supports	86
2.9	Polymers	88
2.9.1	Introduction	88
2.9.2	Polymer Structure.....	89
2.9.2.1	Linear or Chain Polymers.....	89
2.9.2.2	Branched Polymers.....	93
2.9.2.3	Cross-Linked Polymers	93
2.9.3	Furfural Resins.....	95
2.9.4	Coordination Polymers.....	95
	References	97

Chapter 3	Synthesis Methods of Catalyst Adsorbents, Ion Exchangers, and Permeable Materials	103
3.1	Introduction	103
3.1.1	Nucleation and Growth: Johnson–Mehl–Avrami Equation	103
3.2	Methods for the Preparation of Metallic-Supported Catalysts	105
3.2.1	Deposition of the Active Component	105
3.2.1.1	Impregnation.....	105
3.2.1.2	Grafting	106
3.2.1.3	Precipitation.....	106
3.2.1.4	Bifunctional Zeolite Catalysts	107
3.2.1.5	Chemical Vapor Deposition.....	107
3.2.1.6	Case Study: Preparation of Ni Bifunctional Catalysts Supported on Homoionic: Na, K, Ca, and Mg Clinoptilolite	108
3.3	Synthesis of Inorganic Solids	110
3.3.1	Solid-State Reaction Method	110
3.3.2	Solgel Methodologies	111
3.3.2.1	Introduction	111
3.3.2.2	Pechini Method.....	112
3.3.3	Solgel Route Based on the Hydrolysis–Condensation of Metal Alkoxides.....	112
3.3.4	Acetate Precipitation	115
3.4	Synthesis of Microporous Crystalline Materials.....	116
3.4.1	Aluminosilicate Synthesis.....	116
3.4.2	High-Silica, All-Silica, and Non-Aluminosilicate Zeolites Synthesis.....	116
3.4.3	Hydrothermal Transformation of Clinoptilolite to Produce Zeolites Na-X and Na-Y	117

3.4.4	Synthesis of MeAPO Molecular Sieves	121
3.4.5	Synthesis of Pillared, Layered Crystalline Microporous Materials	122
3.5	Synthesis of Ordered Silica Mesoporous Materials	124
3.6	Active Carbon and Carbon Nanotube Preparation Methods.....	125
3.7	Membrane Preparation Methods	126
3.7.1	Ceramic Method.....	126
3.7.2	Template Leaching	127
3.7.3	Composite Membranes.....	128
3.8	Polymer Synthesis	129
3.8.1	Step-Growth Polymerization.....	129
3.8.2	Chain Reaction or Addition Polymerization	130
	References	130
Chapter 4	Material Characterization Methods	137
4.1	Introduction	137
4.2	Application of XRD in Material Characterization.....	137
4.2.1	Bragg–Brentano Geometry Powder Diffractometer	137
4.2.2	Intensity of a Diffraction Peak of a Powdered Sample	138
4.2.3	Qualitative Identification of Phases.....	138
4.2.4	Rietveld Method	139
4.2.5	Quantitative Phase Analysis.....	141
4.2.6	Lattice Parameter Determination.....	144
4.2.6.1	Examples of the Use of Lattice Parameter Determination in the Study of Materials.....	147
4.2.7	Scherrer–Williamson–Hall Methodology for Crystallite Size Determination.....	147
4.3	Electron Microscopy	148
4.3.1	Introduction	148
4.3.2	Transmission Electron Microscope.....	149
4.3.3	Scanning Electron Microscope	150
4.3.4	SEM Applications	153
4.4	Energy-Dispersive Analysis of X-Rays	154
4.4.1	X-Ray Emission.....	154
4.4.2	Applications of Energy-Dispersive Analysis of X-Rays	156
4.5	Infrared and Raman Spectrometries	157
4.5.1	Introduction	157
4.5.2	Differences and Similarities between IR and Raman Phenomena	158
4.5.3	Molecular Vibrations.....	158
4.5.4	Dipole Moment and Polarization	159
4.5.5	Types of Transitions between States	160
4.5.6	IR and Raman Transition Probabilities.....	162
4.5.7	Selection Rules	163
4.5.8	Simplification of the Molecular Vibration Analysis	165
4.5.9	Instrumentation	166
4.5.9.1	Fourier Transform Infrared Spectrometer.....	166
4.5.9.2	Conventional Raman Spectrometer.....	167
4.5.9.3	Fourier Transform Raman Spectrometer.....	167

4.5.10	Applications of Fourier Transform Infrared Spectroscopy and Raman Spectroscopy in Materials Science	168
4.6	Nuclear Magnetic Resonance Spectrometry	173
4.6.1	Introduction	173
4.6.2	NMR Spectra.....	173
4.6.3	Chemical Shift.....	175
4.6.4	Spin–Spin Coupling	176
4.6.5	Magic Angle Spinning-Nuclear Magnetic Resonance	176
4.6.6	Applications of MAS-NMR.....	177
4.7	Thermal Methods of Analysis.....	179
4.7.1	Differential Thermal Analysis	180
4.7.2	Thermal Gravimetric Analysis.....	181
4.7.3	Differential Scanning Calorimetry	182
4.7.4	Temperature-Programmed Reduction.....	182
4.7.5	Temperature-Programmed Desorption	183
4.7.6	Fourier Transform Infrared-Temperature Programmed Desorption	184
4.8	Dielectric Analysis Methods	187
4.8.1	Introduction	187
4.8.2	Thermodielectric Analyzer	189
4.8.3	Thermodielectric Analysis.....	191
4.8.3.1	First Effect in TDA	191
4.8.3.2	Second Effect in TDA.....	194
4.8.3.3	Third Effect in TDA	194
4.8.4	Dielectric Spectroscopy.....	196
4.9	Mössbauer Spectrometry	201
4.9.1	Introduction	201
4.9.2	Mössbauer Spectrometer	201
4.9.3	Hyperfine Interactions.....	203
4.9.3.1	Chemical or Isomer Shift.....	203
4.9.3.2	Quadrupole Splitting	204
4.9.3.3	Magnetic Splitting	207
4.9.4	Applications of ^{57}Fe Mössbauer Spectrometry.....	208
4.10	Mercury Porosimetry.....	211
4.11	Magnetic Force in Nonuniform Fields: Phase Analysis Method	213
	References	214
Chapter 5	Diffusion in Materials	219
5.1	Introduction	219
5.2	Fick’s Laws	219
5.3	Thermodynamics of Irreversible Processes	220
5.4	Diffusion Coefficients	222
5.4.1	Tracer-Diffusion Coefficient and Self-Diffusion Coefficient	222
5.4.2	Intrinsic Diffusion Coefficient: The Kirkendall Effect.....	223
5.4.3	Interdiffusion or Chemical Diffusion Coefficient.....	226
5.5	Microscopic Description of Diffusion.....	226
5.5.1	Introduction	226
5.5.2	Random Walker in One Dimension	227

5.5.3	Fokker–Planck Equation	228
5.5.4	Diffusion Mechanisms in Crystalline Solids	229
5.5.4.1	Vacancy Mechanism	230
5.5.4.2	Interstitial Mechanism	231
5.5.5	Random Walker in a Cubic Crystalline Structure	232
5.6	Some Diffusion Processes in Metals	234
5.6.1	Hydrogen Diffusion in Metals	234
5.6.2	Formation of a Surface Fe–Ni Alloy	235
5.6.3	Effect of the Diffusion of Fe in a Fe–Ni Alloy during the Oxidation of the Alloy with Nitric Oxide	239
5.7	Diffusion in Oxides	240
5.7.1	Defect Chemistry of Oxides	240
5.7.2	Oxygen Transport in Oxides	243
5.7.3	Defect Chemistry in Proton-Conducting Perovskites	245
5.7.4	Proton Transport Mechanisms	246
5.7.5	Band Structure of Proton-Conducting Perovskites	247
5.7.6	Proton Transport Mechanism in Oxides	247
5.7.7	Absorption and Diffusion of Hydrogen in Nanocrystals of the BaCe _{0.95} Yb _{0.05} O _{3-δ} Proton-Conducting Perovskite	249
5.8	Diffusion in Porous Media	254
5.8.1	Transport Mechanisms in Porous Media	254
5.8.2	Viscous versus Knudsen Flows	256
5.8.3	Viscous Flow in a Straight Cylindrical Pore	257
5.8.4	Knudsen Flow in a Straight Cylindrical Pore	257
5.9	Diffusion in Micropores	258
5.9.1	Mechanism of Diffusion in Zeolites	258
5.9.2	Single-Component Diffusion in Zeolites	263
5.9.3	Two-Component Diffusion in Zeolites	269
	References	271
Chapter 6	Adsorption in Nanoporous Materials	275
6.1	Introduction	275
6.2	Definitions and Terminology	275
6.2.1	Some Definitions	275
6.2.1.1	Adsorption and Desorption	275
6.2.1.2	Pore Size	276
6.2.1.3	Adsorption Space Filling	276
6.2.1.4	Dynamic Adsorption	276
6.2.1.5	Adsorption Isotherm	276
6.2.1.6	Physical and Chemical Adsorptions	276
6.2.1.7	Mobile and Immobile Adsorptions	276
6.2.1.8	Monolayers and Multilayers	276
6.2.1.9	Parameters Characterizing Porous Adsorbents	276
6.2.2	Magnitude of Adsorption	277
6.3	Adsorption Interaction Fields	278
6.4	Measurement of Adsorption Isotherms by the Volumetric Method	282
6.5	Thermodynamics of Adsorption	283
6.5.1	Isosteric and Differential Heats of Adsorption	283
6.5.2	Calorimetry of Adsorption	285

6.5.3	Some Relations between Macroscopic and Microscopic Adsorption Parameters	288
6.6	Systems for the Automatic Measurement of Surface Area and Porosity by the Volumetric Method	290
6.6.1	Equipment	290
6.6.2	Porous Material Characterization by Adsorption Methods	290
6.7	Adsorption in Zeolites	291
6.7.1	Introduction	291
6.7.2	Some Examples of Adsorption Systems in Zeolites	292
6.7.3	Determination of the Micropore Volume	292
6.7.3.1	Dubinin Adsorption Isotherm Equation	292
6.7.3.2	Osmotic Adsorption Isotherm Equation	294
6.7.3.3	Langmuir-Type and Fowler–Guggenheim-Type Adsorption Isotherm Equations	295
6.8	Adsorption in Nanoporous-Ordered and Amorphous Materials	297
6.8.1	Mesoporous Molecular Sieves	297
6.8.2	Amorphous Silica	298
6.8.3	Adsorption in Active Carbon and Carbon Nanotubes	300
6.8.4	Determination of the Specific Surface of Materials	301
6.9	Howarth–Kawazoe Approach for the Description of Adsorption in Microporous Materials for the Slit, Cylindrical, and Spherical Pore Geometries	303
6.10	Adsorption from Liquid Solutions	310
6.10.1	Introduction	310
6.10.2	Isotherms for the Description of Adsorption from Liquid Phase	310
6.11	Dynamic Adsorption: The Plug-Flow Adsorption Reactor	312
6.11.1	Dynamic Adsorption	312
6.11.2	Plug-Flow Adsorption Reactor Model	314
6.12	Some Chemical, Sustainable Energy, and Pollution Abatement Applications of Nanoporous Adsorbents	317
6.12.1	Gas Separation and Cleaning	317
6.12.2	Hydrogen Storage	321
6.12.2.1	Hydrogen Storage in Zeolites	321
6.12.2.2	Hydrogen Storage in Mesoporous Molecular Sieves and Pillared Clays	322
6.12.2.3	Hydrogen Storage in Silica	322
6.12.2.4	Hydrogen Storage in Carbon-Based Adsorbents	324
6.12.3	Methane Storage in Adsorbents	325
6.12.3.1	Introduction	325
6.12.3.2	Methane Storage in Carbonaceous Adsorbents	326
6.12.4	Water Cleaning	327
6.13	Porous Polymers as Adsorbents	329
6.13.1	Porous and Coordination Polymers	329
6.13.2	Applications of Porous Polymers and Coordination Polymers in Adsorption Processes	331
	References	333
Chapter 7	Ion Exchange	339
7.1	Introduction	339
7.2	Aluminosilicate Zeolite Ion Exchangers	339
7.3	Some Definitions and Terms	340

7.4	Thermodynamics of Ion Exchange.....	342
7.5	Rules Governing the Ion-Exchange Equilibrium in Zeolites	344
7.5.1	Regular Systems	344
7.5.2	Space Limitations and Molecular Sieving	344
7.5.3	Irregular Systems	345
7.5.4	Systems with Phase Transformations.....	345
7.5.5	Electroselectivity	345
7.5.6	Effect of pH of the Electrolytic Solution on the Ion-Exchange Process	345
7.6	Ion-Exchange Heat	346
7.6.1	Ion-Exchange Heat Measurement	346
7.7	Ion-Exchange Selectivity in Zeolites.....	349
7.8	Ion-Exchange Kinetics	350
7.8.1	Interdiffusion in the Adhering Liquid Thin Layer as the Limiting Step.....	350
7.8.2	Interdiffusion of A and B in Zeolite Crystals as the Limiting Step	352
7.8.3	Experimental Results	353
7.9	Plug-Flow Ion-Exchange Bed Reactors.....	353
7.9.1	Introduction	353
7.9.2	Parameters for the Design of a Laboratory PFIER.....	355
7.10	Chemical and Pollution Abatement Applications of Ion Exchange in Zeolites	355
7.10.1	Introduction	355
7.10.2	Heavy Metal Removal from Wastewater	356
7.10.3	Recovery of Ni ²⁺ from the Waste Liquors of a Nickel Production Plant.....	361
7.10.4	Municipal Wastewater Treatment.....	361
7.10.5	Radioactive Wastewater Treatment	362
7.10.6	Catalytic Effect of Proton Exchange in Natural Zeolites in Biogas Production During Anaerobic Digestion.....	363
7.10.7	Zeolite Na-A as Detergent Builder.....	364
7.10.8	Aquaculture	364
7.11	Applications of Other Crystalline Inorganic Ion Exchangers	365
7.11.1	Hydrotalcites	365
7.11.2	Sodium Titanates.....	366
7.11.3	Titanium Silicates.....	366
7.11.4	Zirconium Phosphates.....	367
7.12	Ion-Exchange Polymeric Resins.....	367
7.12.1	General Characteristics of Ion-Exchange Resins	367
7.12.2	Ion-Exchange Resin Swelling	368
7.12.3	Applications of Ion-Exchange Polymeric Resins	370
	References	371
Chapter 8	Solid-State Electrochemistry	375
8.1	Introduction	375
8.1.1	Batteries and Fuel Cells.....	375
8.1.2	Types of Fuel Cells.....	375
8.1.2.1	Polymer Electrolyte Fuel Cell.....	376
8.1.2.2	Alkaline Fuel Cell	377
8.1.2.3	Phosphoric Acid Fuel Cell	378

	8.1.2.4 Molten Carbonate Fuel Cell.....	379
	8.1.2.5 Solid Oxide Fuel Cell	380
8.2	Solid Electrolytes.....	380
	8.2.1 Defect Concentration in Ionic Compounds	381
	8.2.2 Unipolar Ionic Conductivity in Solids.....	381
	8.2.3 Examples of Unipolar Cationic Conductors.....	384
	8.2.4 Anionic Conductors.....	385
	8.2.5 Proton Conductors.....	385
	8.2.5.1 Introduction	385
	8.2.5.2 Conductivity in Proton Conductors	385
	8.2.6 Oxide Conduction.....	386
	8.2.6.1 Oxygen Conductors	386
	8.2.6.2 Conductivity in Oxygen Conductors.....	388
	8.2.7 Zeolite Electrolyte.....	389
8.3	Thermodynamics of Electrochemical Processes.....	392
8.4	Kinetics of Electrochemical Processes	393
	8.4.1 Overpotential.....	393
	8.4.2 Activation Polarization.....	394
	8.4.2.1 Tafel Equation.....	394
	8.4.2.2 Calculation of the Transference Coefficient	395
	8.4.3 Ohmic Polarization	398
	8.4.4 Concentration Polarization.....	398
8.5	Fuel Cell Efficiency	398
	8.5.1 Polarization Curve.....	398
	8.5.2 Thermodynamic Efficiency of a Fuel Cell.....	399
	8.5.3 Electrochemical Efficiency of a Fuel Cell.....	400
	8.5.4 Efficiency of an Internal Combustion Engine	401
8.6	Electrochemical Impedance Spectroscopy	401
	8.6.1 Impedance Analysis	401
	8.6.2 Dielectric Spectroscopy and Impedance Spectroscopy	402
	8.6.3 Equivalent Circuits for Electrochemical Cells	404
	8.6.4 Methods for the Representation of Impedance Spectroscopy Data.....	405
8.7	Sustainable Energy and Environmental Sensing Technology	
	Applications of Solid-State Electrochemistry	407
	8.7.1 Solid Oxide Fuel Cell Materials and Performance	407
	8.7.1.1 Electrolyte.....	407
	8.7.1.2 SOFC Cathode Materials and Performance	408
	8.7.1.3 SOFC Anode Materials and Performance	409
	8.7.1.4 Interconnects.....	410
	8.7.1.5 SOFC Fuel Processing.....	410
	8.7.2 Polymer Electrolyte Fuel Cells.....	412
	8.7.2.1 Electrolyte.....	412
	8.7.2.2 Electrodes	413
	8.7.3 Zeolites as Solid Electrolytes in Batteries.....	413
	8.7.4 Sensors	414
	References	416

Chapter 9 Heterogeneous Catalysis and Surface Reactions

9.1	Introduction	421
9.2	General Properties of Catalysts.....	421

9.3	Crystalline and Ordered Nanoporous Heterogeneous Catalysts	423
9.3.1	Acid Zeolite Catalysts: Brönsted Type.....	423
9.3.2	Bifunctional Zeolite Catalysts.....	425
9.3.3	Acid Zeolite Catalysts: Lewis Type	425
9.3.4	Basic Zeolite Catalysts	425
9.3.5	Catalysts Obtained by the Isomorphous Substitution of Ti in Zeolites	426
9.3.6	Pillared Clays	426
9.3.7	Mesoporous Molecular Sieves.....	428
9.4	Amorphous, Porous Heterogeneous Catalysts and Supports	428
9.4.1	Amorphous Acid Silica–Alumina.....	428
9.4.2	Metallic Catalysts Supported on Amorphous Materials.....	429
9.5	Photocatalysts	430
9.5.1	Introduction	430
9.5.2	Titanium Oxide	430
9.5.3	Other Photocatalysts.....	431
9.6	Kinetics of Surface Reactions	431
9.6.1	Steps in a Heterogeneous Catalytic Reaction.....	431
9.6.2	Reaction Rate	432
9.6.3	Unimolecular Decomposition	433
9.6.4	Calculation of the Adsorption Enthalpy of <i>n</i> -Paraffins in Nanoporous Crystalline and Ordered Acid Catalysts, and Its Relation with the Activation Energy of the Monomolecular Catalytic Cracking Reaction	435
9.6.4.1	Introduction	435
9.6.4.2	Unimolecular Catalytic Cracking.....	436
9.6.4.3	Calculation of the Adsorption Enthalpy	436
9.6.4.4	Calculation of the Activation Energy	438
9.6.4.5	Numerical Evaluation of the Model.....	440
9.6.5	Bimolecular Reaction.....	441
9.6.5.1	Langmuir–Hinshelwood Mechanism	441
9.6.5.2	Eley–Rideal Mechanism.....	442
9.6.6	Composite Mechanism Reactions	443
9.7	Examples of Surface Reactions	444
9.7.1	Reaction between Nitric Oxide and the Surface of Iron	444
9.7.2	Reaction between Carbon Monoxide and the Surface of Nickel	447
9.8	Packed Bed Plug-Flow Catalytic Reactor.....	449
9.8.1	Laboratory Scale Reactor.....	449
9.8.2	Equations Governing the Plug-Flow Packed Bed Reactor.....	450
9.8.3	Solution of the Governing Equation for the First-Order Chemical Reaction	451
9.8.4	Steps in a Catalytic Reaction in a Packed-Bed Reactor.....	452
9.9	Chemical, Sustainable Energy, and Pollution Abatement Applications of Heterogeneous Catalysts	453
9.9.1	Ammonia Synthesis	453
9.9.2	Catalytic Cracking of Hydrocarbons.....	454
9.9.3	Decomposition of Ammonia for Hydrogen Production and Other Applications	454
9.9.4	Fischer–Tropsch Synthesis	455

9.9.5	Water–Gas Shift Reaction for Hydrogen Production and Other Applications	455
9.9.6	Ethanol Dehydration	456
9.9.7	Oxidation of CO	458
9.9.8	Water Treatment by Heterogeneous Photocatalysis	459
9.9.9	Other Sources of Activation of a Photocatalyst Mechanical Activation	459
9.9.10	Hydrogen Production by Photocatalytic Water Splitting	460
9.9.10.1	Solar Water Splitting with Quantum Boost	460
9.9.11	Hydrogen Production by Steam-Reforming of Ethanol	461
9.9.12	Porous Polymers as Catalysts.....	462
	References	462
Chapter 10	Membranes.....	467
10.1	Introduction	467
10.2	Definitions and Nomenclature.....	467
10.2.1	Some Definitions	467
10.2.2	Membrane Unit.....	468
10.2.3	Permeance and Permeability	468
10.2.4	Selectivity	469
10.3	Permeability in Dense Membranes	470
10.3.1	Hydrogen Transport in Metallic Dense Membranes	470
10.3.2	Hydrogen Permeation in Oxide Ceramic Membranes.....	471
10.3.3	Permeation in Dense Oxide Membranes	473
10.4	Permeation in Porous Membranes.....	474
10.4.1	Introduction	474
10.4.2	Transport Mechanisms in Porous Membranes	474
10.4.3	Viscous and Knudsen Flows.....	475
10.4.4	Darcy’s Law for Viscous Flow	475
10.4.5	Darcy’s Law for Knudsen Flow	477
10.4.6	Transport in Zeolite Membranes	477
10.4.7	Zeolite-Based Membranes.....	478
10.4.8	Permeation Flow in Zeolite Membranes	478
10.5	Zeolite-Based Ceramic Porous Membrane	480
10.5.1	Carbon Dioxide Permeation in a Zeolite-Based Ceramic Porous Membrane	480
10.5.2	In Situ Synthesis of an AlPO ₄ -5 Zeolite over a Ceramic Porous Membrane.....	482
10.6	Chemical, Sustainable Energy, and Pollution Abatement Applications of Inorganic Membranes	483
10.6.1	Hydrogen and Oxygen Separations	483
10.6.1.1	Hydrogen Separations.....	483
10.6.1.2	Oxygen Separations.....	484
10.6.2	Catalytic Membrane Reactors	484
10.7	Examples of Polymeric Membranes.....	485
	References.....	487
	Index.....	491

Preface

Since ancient times, the development and use of materials has been one of the basic objectives of mankind. Eras, that is, the Stone Age, the Bronze Age, and the Iron Age, have been named after the fundamental material used by mankind to construct their tools. Materials science is the modern activity that provides the raw material for this endless need, demanded by the progress in all fields of industry and technology, of new materials for the development of society.

Metallurgy was one of the first fields where material scientists worked toward developing new alloys for different applications. During the first years, a large number of studies were carried out on the austenite–martensite–cementite phases achieved during the phase transformations of the iron–carbon alloy, which is the foundation for steel production, later the development of stainless steel, and other important alloys for industry, construction, and other fields was produced.

Later, the evolution of the electronic industry initiated the development of an immense variety of materials and devices based, essentially, on the properties of semiconductor, dielectric, ferromagnetic, superconductor, and ferroelectric materials.

In addition, until the second half of the twentieth century, the term ceramic was related to the traditional clays, that is, pottery, bricks, tiles, and cements and glass; however, during the last 50 years, the field of technical ceramics has been rapidly developed, and firmly established.

At the beginning of the twentieth century, the first synthetic polymer, bakelite, was obtained and later, after the First World War, it was proposed that polymers consisted of long chains of atoms held together by covalent bonds. The Second World War gave a huge stimulus to the creation of polymers, which firmly established the field of polymers.

However, important groups of materials cannot be studied in a single volume materials science book. These materials include adsorbents, ion exchangers, ion conductors, catalysts, and permeable materials. Examples of these types of materials are perovskites, zeolites, mesoporous molecular sieves, silica, alumina, active carbons, titanium dioxide, magnesium oxide, clays, pillared clays, hydrotalcites, alkali metal titanates, titanium silicates, polymers, and coordination polymers. These materials have applications in many fields, among others, adsorption, ion conduction, ion exchange, gas separation, membrane reactors, catalysts, catalytic supports, sensors, pollution abatement, detergents, animal nutrition, agriculture, and sustainable energy applications.

The author of this book has been permanently active during his career in the field of materials science, studying diffusion, adsorption, ion exchange, cationic conduction, catalysis and permeation in metals, zeolites, silica, and perovskites. From his experience, the author considers that during the last years, a new field in materials science, that he calls the “physical chemistry of materials,” which emphasizes the study of materials for chemical, sustainable energy, and pollution abatement applications, has been developed. With regard to this development, the aim of this book is to teach the methods of syntheses and characterization of adsorbents, ion exchangers, cationic conductors, catalysts, and permeable porous and dense materials and their properties and applications.

Rolando M.A. Roque-Malherbe

Las Piedras, PR, USA

January, 2009

Author



Dr. Rolando M. A. Roque-Malherbe was born in 1948 in Güines, Havana, Cuba. He graduated with a BS in physics from the University of Havana (1970), *summa cum laude*, specialized (MS equivalent degree) in surface physics at the National Center for Scientific Research, Technical University of Dresden, Germany (1972), *magna cum laude*, and obtained his PhD in physics (solid state physics) from the Moscow Institute of Steel and Alloys, Russia (1978), *magna cum laude*. He completed postdoctoral stints at the Technical University of Dresden, Germany; Moscow State University, Russia; the Technical University of Budapest, Hungary; the Institute of Physical Chemistry and Chemical Physics, Russian Academy of Science, Moscow; and the Central Research Institute for Chemistry, Hungarian Academy of Science, Budapest (1978–1984). The group led by him at the National Center for Scientific Research, Higher Pedagogical Institute, Varona, Havana, Cuba (1980–1992), was one of the world leaders in the study and applications of natural zeolites. During this period, he was possibly the only Cuban scientist to receive most awards. In 1993, after a political confrontation with the Cuban regime, he left Cuba with his family as a political refugee. From 1993 to 1999, he worked at various institutions like the Institute of Chemical Technology, Valencia, Spain; at Clark Atlanta University, Atlanta, Georgia; and at Barry University, Miami, Florida. From 1999 to 2004, he was dean and full professor at the School of Sciences in the University of Turabo, Gurabo, Puerto Rico, and currently he is the director of the Institute of Physical and Chemical Applied Research. He has published 121 papers, 5 books, 6 chapters, 30 abstracts, has 15 patents, and made more than 200 presentations at scientific conferences. He is currently an American citizen.

1 Materials Physics

1.1 INTRODUCTION

We discuss briefly some basic topics in materials physics such as crystallography, lattice vibrations, band structure, x-ray diffraction, dielectric relaxation, nuclear magnetic resonance and Mössbauer effects in this chapter. These topics are an important part of the core of this book. Therefore, an initial analysis of these topics is useful, especially for those readers who do not have a solid background in materials physics, to understand some of the different problems that are examined later in the rest of the book.

1.2 CRYSTALLOGRAPHY

1.2.1 CRYSTALLINE STRUCTURE

An unit cell is a regular repeating pattern that pervades the whole crystal lattice. It is described [1–6] by three vectors: \bar{a} , \bar{b} , and \bar{c} (Figure 1.1), that outline a parallelepiped, characterized by six parameters. These parameters are the length of the three vectors (a , b , and c) and the angles between them (α , β , and γ). Consequently, all the points that constitute the lattice sites are given by a set of points, which starting from a reference point, are given by

$$\bar{R} = n_1\bar{a} + n_2\bar{b} + n_3\bar{c} \quad (1.1)$$

where n_1 , n_2 , n_3 , are integers running from $-\infty$ to ∞ , for a limitless crystal. As a result of this, the lattice is a set of points in space, distinguished by a space periodicity or a translational symmetry. This means that under a translation defined by Equation 1.1, the lattice remains invariant.

If all the lattice points are positioned in the eight corners of a unit cell, then the unit cell is called a primitive unit cell. However, often, for convenience, larger unit cells, which are not primitives, are selected for the description of a particular lattice, as will be explained later.

It is possible, as well, to define the primitive unit cell, by surrounding the lattice points, by planes perpendicularly intersecting the translation vectors between the enclosed lattice point and its nearest neighbors [2,3]. In this case, the lattice point will be included in a primitive unit cell type, which is named the Wigner–Seitz cell (see Figure 1.2).

A concrete building procedure in three dimensions of the Wigner–Seitz cell can be achieved by representing lines from a lattice point to others in the lattice and then drawing planes that cut in half each of the represented lines, and finally taking the minimum polyhedron enclosing the lattice point surrounded by the constructed planes.

Till now, we have only considered a mathematical set of points. However, a material, in reality, is not merely an array of points, but the group of points is a lattice. A real crystalline material is constituted of atoms periodically arranged in the structure, where the condition of periodicity implies a translational invariance with respect to a translation operation, and where a lattice translation operation, \bar{T} , is defined as a vector connecting two lattice points, given by Equation 1.1 as

$$\bar{T} = n_1\bar{a} + n_2\bar{b} + n_3\bar{c} \quad (1.2)$$

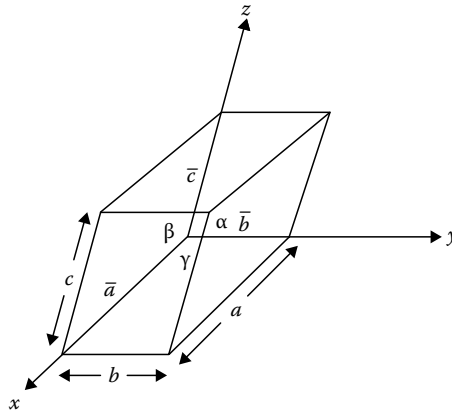


FIGURE 1.1 Unit cell geometrical representation.

Until now, we have considered an infinite lattice, but a real material has limited dimensions, that is, n_1, n_2, n_3 has boundaries. However, an infinite array of unit cells is a good approximation for regions relatively far from the surface, which constitutes the major part of the whole material [5]. At this point, it is necessary to recognize that a real crystal has imperfections, such as vacancies, dislocations, and grain boundaries.

Since a lattice is just a set of points, we will need another entity to describe the real crystal. That is, it is required to locate a set of atoms named “basis” in the vicinity of the lattice sites. Therefore, a crystal will be a combination of a lattice and a basis of atoms. In Figure 1.3, a representation of the operation

$$\text{lattice} + \text{basis} = \text{crystal}$$

is given.

In order to systematize in a logical form the lattices that are compatible with a periodicity condition, the French physicist Auguste Bravais, in 1845, demonstrated that the lattice points in three dimensions, congruent with the periodicity requirement, are the roots of the following trigonometric equation [2]:

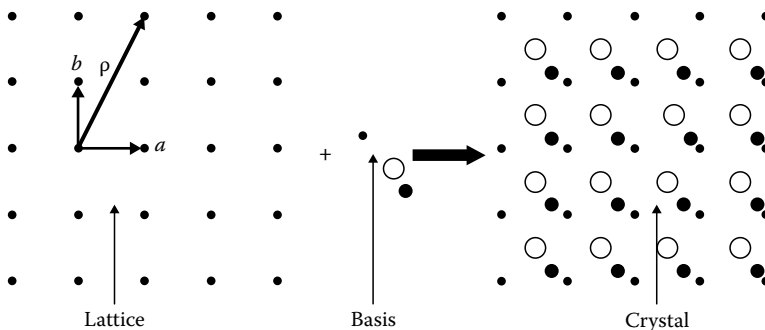


FIGURE 1.3 Representation of the operation: lattice + basis = crystal.

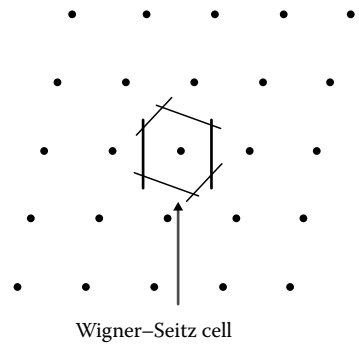


FIGURE 1.2 Wigner–Seitz cell in two dimensions.

TABLE 1.1
Description of the Seven Crystalline Systems

System	Parameters Describing the Unit Cell
Cubic	$a = b = c; \alpha = \beta = \gamma = 90^\circ$
Hexagonal	$a = b \neq c; \alpha = \beta = 90^\circ; \gamma = 120^\circ$
Rhombohedral or trigonal	$a = b = c; \alpha = \beta = \gamma \neq 90^\circ$ and $<120^\circ$
Tetragonal	$a = b \neq c; \alpha = \beta = \gamma = 90^\circ$
Orthorhombic	$a \neq b \neq c; \alpha = \beta = \gamma = 90^\circ$
Monoclinic	$a \neq b \neq c; \alpha = \beta = 90^\circ \neq \gamma$
Triclinic	$a \neq b \neq c; \alpha \neq \beta \neq \gamma \neq 90^\circ$

$$\sin^2 \left[\frac{\pi \xi}{a} \right] + \sin^2 \left[\frac{\pi \eta}{b} \right] + \sin^2 \left[\frac{\pi \zeta}{c} \right] = 0 \quad (1.3)$$

where

ξ , η , and ζ are spatial coordinates related with an oblique three-coordinate axis system
 \bar{a} , \bar{b} , and \bar{c} (see Figure 1.1) are the unit vectors of the coordinate system

Bravais then showed that in three dimensions, there are only 14 different lattice types, currently named the Bravais lattices, which are grouped in seven crystal systems [1–3] (see Table 1.1).

Each lattice has an inversion center, a unique set of axes and symmetry planes, and there are possible operations like rotation, reflection, and its combinations [1]. In a case where some symmetry operations leave unchanged a particular point of the fixed lattice, they form a group called the crystallographic point groups. In this regard, there are 32 point groups in three dimensions. Besides, the combination of the point group symmetry operations with the translation symmetry gives rise to the crystallographic space groups. In relation with these operations, there are 230 space groups in three dimensions [1].

Each crystal system is related with a parallelepiped whose vertices are compatible with the sites of the corresponding Bravais lattice (see Figure 1.4) [1–3]. The parallelepiped is described with six parameters, as was previously stated for the unit cell. The most symmetrical crystal system has an essential symmetry, 4 threefold axes, and is named the cubic system. A hexagonal lattice is characterized completely by a regular hexahedral prism, having a sixfold axes as the essential symmetry. This crystal system is named the hexagonal system. The Bravais trigonal lattice is characterized by a geometrical figure that results when a cube is stretched along one of its diagonals (see Figure 1.4). In addition, a rectangular prism with at least one square face has a tetragonal symmetry, that is, a fourfold axes as the essential symmetry, and is the basis of the tetragonal system. Stretching the tetragonal prism along one of the axes produces the orthorhombic prism, having three orthogonal twofold axes as the essential symmetry, and is the origin of the orthorhombic system. To complete the seven crystal systems, it is necessary to include the monoclinic system, which has only a twofold axes as the essential symmetry, and the triclinic system, which has only an inversion center.

Within a given crystal system, a supplementary subdivision is necessary to be made, in order to produce the 14 Bravais lattices. In this regard, it is necessary to make a distinction between the following types of Bravais lattices, that is, primitive (P) or simple (S), base-centered (BC), face-centered (FC), and body-centered (BoC) lattices [1–3].

In Table 1.2, the subtypes corresponding to each crystal system are listed and in Figure 1.4, the 14 Bravais lattices in three dimensions are illustrated.

Among the 14 cells that generate the Bravais lattices (see Figure 1.4), only the P-type cells are considered primitive unit cells. It is possible to generate the other Bravais lattices with primitive unit cells. However, in practice, only unit cells that possess the maximum symmetry are chosen (see Figure 1.4 and Table 1.2) [1–6].

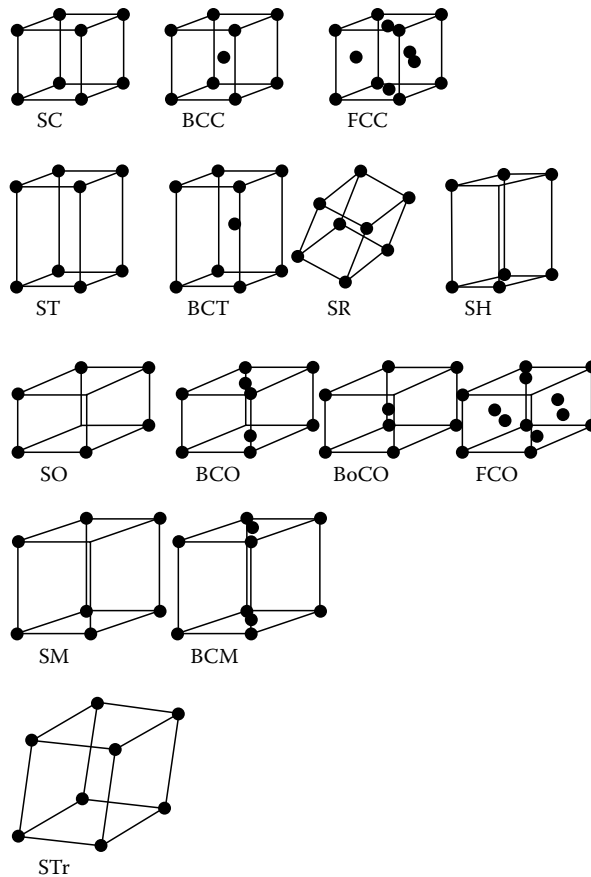


FIGURE 1.4 Bravais lattices.

TABLE 1.2
Subtypes of Lattices in the Seven Crystalline Systems

System	Lattice Types
Cubic	Simple cubic (SC), body-centered cubic (BCC), and face-centered cubic (FCC)
Hexagonal	Simple hexagonal (SH)
Rhombohedral or trigonal	Simple rhombohedral (SR)
Tetragonal	Simple tetragonal (ST) and body-centered tetragonal (BCT)
Orthorhombic	Simple orthorhombic (SO), body-centered orthorhombic (BoCO), face-centered orthorhombic (FCO), and base-centered orthorhombic (BCO)
Monoclinic	Simple monoclinic (SM) and base-centered monoclinic (BCM)
Triclinic	Simple triclinic (STr)

Sources: Schwarzenbach, D., *Crystallography*, John Wiley & Sons, New York, 1997; Kittel, Ch., *Introduction to Solid State Physics*, 8th edn., John Wiley & Sons, New York, 2004; Myers, H.P., *Introduction to Solid State Physics*, 2nd edn., CRC Press, Boca Raton, FL, 1997.

1.2.2 CRYSTALLOGRAPHIC DIRECTIONS AND PLANES

The following steps must be followed in order to specify a crystallographic direction:

1. The vector that defines the crystallographic direction should be situated in such a way that it passes through the origin of the lattice coordinate system.
2. The projections of this vector on each of the three axis is determined and measured in terms of the unit cell dimensions, a , b , c , obtaining three integer numbers, n_1 , n_2 , n_3 .
3. These numbers are reduced to smallest integers, u , v , w .
4. These three numbers, enclosed in square brackets and not separated with commas, $[uvw]$, denote the crystallographic direction.

For example, the direction of the positive x -axis is denoted by $[100]$, the direction of the positive y -axis is denoted by $[010]$, and the direction of the positive z -direction is denoted by $[001]$ (see Figure 1.1).

For a crystal having a hexagonal symmetry, a set of four numbers, $[uv tw]$, named the Miller–Bravais coordinate system (see Figure 1.5), is used to describe the crystallographic directions, where the first three numbers, that is, u , v , t , are projections along the axes a_1 , a_2 , and a_3 , describing the basal plane of the hexagonal structure, and w is the projection in the z -direction [2,3].

The following steps should be followed in order to specify a crystallographic plane:

1. The plane ought to be located in such a way that it does not pass through the origin of the lattice coordinate system.
2. After this, the interceptions of the plane on each of the three axis is determined in terms of the unit cell dimensions, a , b , c , and then obtaining three integer numbers p_1 , p_2 , p_3 .
3. The reciprocals of these numbers are then taken and thereafter reduced to smallest integers h , k , l .
4. These three numbers enclosed in parentheses and not separated with commas, that is, (hkl) , named the Miller indexes, denote the crystallographic plane.

For example, the plane perpendicular to the x -axis is denoted by (100) , the plane perpendicular to the y -axis is denoted by (010) , and the plane perpendicular to the positive z -direction is denoted by (001) .

For a crystal exhibiting a hexagonal symmetry, a set of four numbers, $(hkil)$, (see Figure 1.5) is used to describe the crystallographic planes, where the first three numbers, that is, h , k , i , are the intercepts of the plane on each of the three axis measured in terms of the unit cell dimensions along the axes a_1 , a_2 , and a_3 , describing the basal plane of the hexagonal structure, and l is the projection in the z -direction.

The position of a point inside the primitive unit cell is determined by a fraction of the axial length, a , b , c . For example, in a body-centered structure, the position of the central point is $\frac{1}{2} \frac{1}{2} \frac{1}{2}$.

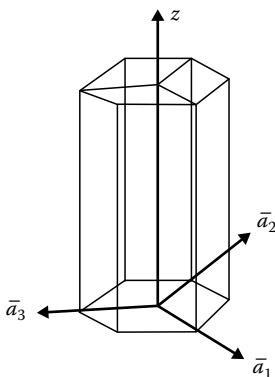


FIGURE 1.5 Miller–Bravais coordinate system.

1.2.3 OCTAHEDRAL AND TETRAHEDRAL SITES IN THE FCC LATTICE

In the FCC lattice, two types of interstitial sites can be recognized: octahedral sites (O-sites) and tetrahedral sites (T-sites). The O-sites are those which are enclosed by six nearest neighbor atoms at the same distances (see Figure 1.6).

On the other hand, a T-site is the geometric place that is formed when three spheres are in contact with each other, and a fourth sphere is placed in the depression created by the first three. In this case, a tetrahedral site is formed in between the four spheres. That is, if we join three small black spheres located in the centers of the faces (see Figure 1.7), surrounding the diagonal of the cube, we will construct a triangle.

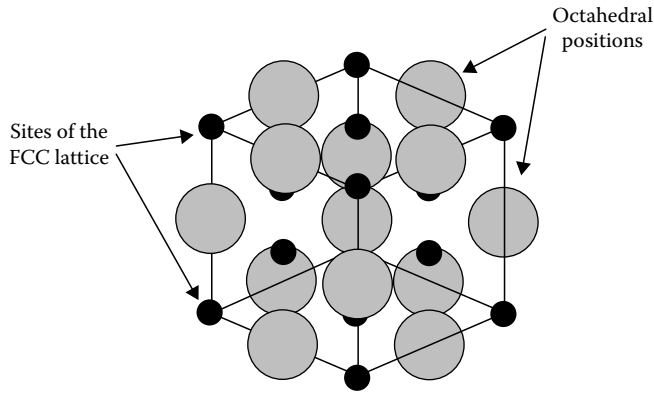


FIGURE 1.6 Octahedral sites.

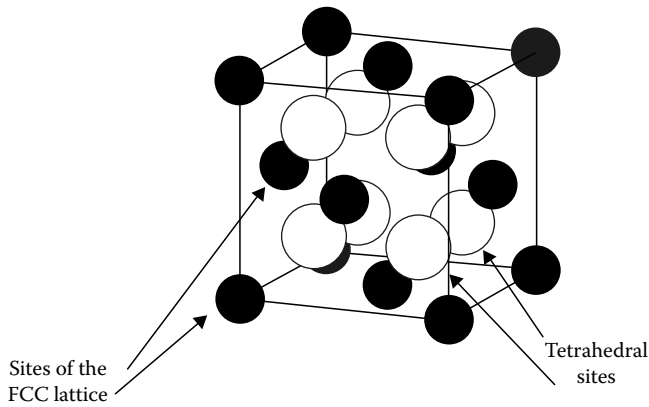


FIGURE 1.7 Tetrahedral sites.

1.2.4 RECIPROCAL LATTICE

A unit cell in the reciprocal lattice is described by the vectors \bar{a}^* , \bar{b}^* , \bar{c}^* , which are defined as follows [2,3,5,6]:

$$\bar{a}^* = 2\pi \frac{\bar{b} \times \bar{c}}{V}, \quad \bar{b}^* = 2\pi \frac{\bar{c} \times \bar{a}}{V}, \quad \text{and} \quad \bar{c}^* = 2\pi \frac{\bar{a} \times \bar{b}}{V} \quad (1.4)$$

where $V = \bar{a} \cdot (\bar{b} \times \bar{c})$

Hence,

$$\bar{a} \cdot \bar{a}^* = \bar{b} \cdot \bar{b}^* = \bar{c} \cdot \bar{c}^* = 2\pi \quad (1.5a)$$

and

$$\bar{a} \cdot \bar{b}^* = \bar{a} \cdot \bar{c}^* = \bar{b} \cdot \bar{a}^* = \bar{b} \cdot \bar{c}^* = \bar{c} \cdot \bar{a}^* = \bar{c} \cdot \bar{b}^* = 0 \quad (1.5b)$$

This means that \bar{a}^* is perpendicular to both \bar{b} and \bar{c} , \bar{b}^* is perpendicular to both \bar{a} and \bar{c} , and \bar{c}^* is perpendicular to both \bar{b} and \bar{a} .

Similar to the direct lattice, all the possible points that lie at the reciprocal lattice can be represented as follows:

$$\overline{G}_{hkl} = h\overline{a}^* + k\overline{b}^* + l\overline{c}^* \quad (1.6)$$

Now, since the Miller indices of a plane implies that the plane intercepts the base vectors at the point $\frac{\overline{a}}{h}, \frac{\overline{b}}{k}, \frac{\overline{c}}{l}$, a triangular portion of the plane has sides

$$\left(\frac{\overline{a}}{h} - \frac{\overline{b}}{k}\right), \left(\frac{\overline{b}}{k} - \frac{\overline{c}}{l}\right), \left(\frac{\overline{c}}{l} - \frac{\overline{a}}{h}\right)$$

Considering Equations 1.5, it is possible to show that

$$\left(\frac{\overline{a}}{h} - \frac{\overline{b}}{k}\right) \cdot \overline{G}_{hkl} = \left(\frac{\overline{b}}{k} - \frac{\overline{c}}{l}\right) \cdot \overline{G}_{hkl} = \left(\frac{\overline{c}}{l} - \frac{\overline{a}}{h}\right) \cdot \overline{G}_{hkl} = 0$$

Consequently, the vector $\overline{G}_{hkl} = \overline{G}_{hkl}$ is perpendicular to the plane (hkl) . Then, it is possible to calculate $|\overline{G}_{hkl}|$, that is, the vector modulus. To perform this calculation, we must define the unit vector in the direction of the vector \overline{G}_{hkl} as follows:

$$\overline{n}_{hkl} = \frac{\overline{G}_{hkl}}{|\overline{G}_{hkl}|}$$

Subsequently, since by definition the interplanar distance, that is, the distance between the (hkl) planes, is

$$d_{hkl} = \frac{\overline{a}}{h} \cdot \overline{n}_{hkl} = \frac{\overline{a}}{h} \cdot \frac{\overline{G}_{hkl}}{|\overline{G}_{hkl}|} = \frac{2\pi}{|\overline{G}_{hkl}|}$$

Consequently,

$$d_{hkl} = \frac{2\pi}{|\overline{G}_{hkl}|} \quad (1.7)$$

1.3 BLOCH THEOREM

The Bloch theorem is one of the tools that helps us to mathematically deal with solids [5,6]. The mathematical condition behind the Bloch theorem is the fact that the equations which governs the excitations of the crystalline structure such as lattice vibrations, electron states and spin waves are periodic. Then, to solve the Schrödinger equation for a crystalline solid where the potential is periodic, $\{V(\vec{r} + \vec{R}) = V(\vec{r})\}$, this theorem is applied [5,6].

If $V(\vec{r})$ is the potential “seen” by an electron belonging to the solid, then the one electron wave function, $\psi(\vec{r})$, satisfies the Schrödinger equation:

$$-\frac{\hbar^2}{2m}\nabla^2\psi(\vec{r})+V(\vec{r})\psi(\vec{r})=E\psi(\vec{r}) \quad (1.8)$$

In the case of lattice waves and spin waves, the procedure is different but the principle is the same. The periodic potential is represented with the help of a Fourier series

$$V(\vec{r})=\sum_{\vec{G}_{hkl}}V_{\vec{G}_{hkl}}e^{i\vec{G}_{hkl}\cdot\vec{r}}$$

where $\vec{G}_{hkl}=\vec{d}_{hkl}^*=h\vec{a}^*+k\vec{b}^*+l\vec{c}^*$ is the reciprocal lattice vector. Since $V(\vec{r})$ is a real function, it is necessary that

$$V_{\vec{G}_{hkl}}^*=V_{-\vec{G}_{hkl}}$$

since

$$V^*(\vec{r})=\sum_{\vec{G}_{hkl}}V_{\vec{G}_{hkl}}e^{-i\vec{G}_{hkl}\cdot\vec{r}}=\sum_{\vec{G}_{hkl}}V_{-\vec{G}_{hkl}}e^{i\vec{G}_{hkl}\cdot\vec{r}}=V(\vec{r})$$

Given that the Schrödinger equation

$$\left(-\frac{\hbar^2}{2m}\nabla^2+V(\vec{r})-E\right)\psi(\vec{r})=(\hat{H}(\vec{r})-E)\psi(\vec{r})$$

is periodic, that is,

$$(\hat{H}(\vec{r})-E)\psi(\vec{r})=(\hat{H}(\vec{r}+\vec{R})-E)\psi(\vec{r}+\vec{R})$$

Then, the wave function $\psi(\vec{r})$ and the wave function $\psi(\vec{r}+\vec{R})$ must differ only in a constant, then

$$\psi(\vec{r}+\vec{R})=\vartheta_{\vec{R}}\psi(\vec{r})$$

where the condition of normalization required by all the wave functions requires that

$$|\vartheta_{\vec{R}}|^2=1$$

Consequently,

$$\vartheta_{\vec{R}}=e^{-i\alpha(\vec{R})}$$

where $\alpha(\vec{R})$ is a real number. Besides, since

$$\vartheta_{\vec{R}_1}\vartheta_{\vec{R}_2}=\vartheta_{\vec{R}_1+\vec{R}_2}$$

we will then have that

$$\alpha(\bar{R}_1) + \alpha(\bar{R}_2) = \alpha(\bar{R}_1 + \bar{R}_2)$$

Subsequently,

$$\alpha(\bar{R}) = \bar{k} \cdot \bar{R}$$

and

$$\vartheta_{\bar{R}} = e^{-i\bar{k} \cdot \bar{R}}$$

$$\Psi(\bar{r} + \bar{R}) = e^{-i\bar{k} \cdot \bar{R}} \Psi(\bar{r})$$

Therefore, the periodic function

$$u(\bar{r}) = e^{-i\bar{k} \cdot \bar{r}} \Psi(\bar{r})$$

Have the correct form to be a solution of Equation 1.8. As a result, the Bloch theorem affirms that the solution to the Schrödinger equation may be a plane wave multiplied by a periodic function, that is [5,6],

$$\Psi_{\bar{k}}(\bar{r}) = e^{i\bar{k} \cdot \bar{r}} u_{\bar{k}}(\bar{r}) \quad (1.9a)$$

where the periodic function is given by

$$u_{\bar{k}}(\bar{r}) = \sum_{\bar{G}_{hkl}} u_{\bar{G}_{hkl}}(\bar{k}) e^{i\bar{G}_{hkl} \cdot \bar{r}} \quad (1.9b)$$

It is necessary to state now that the rigorous fulfillment of the Bloch theorem needs an infinity lattice. In order to calculate the number of states in a finite crystal, a mathematical requirement named the Born–Karman cyclic boundary condition is introduced. That is, if we consider that a crystal with dimensions $N_1\bar{a}$, $N_2\bar{b}$, $N_3\bar{c}$ is cyclic in three dimensions, then [5]

$$\Psi(\bar{r} + N_1\bar{a}) = \Psi(\bar{r}), \quad \Psi(\bar{r} + N_2\bar{b}) = \Psi(\bar{r}), \quad \text{and} \quad \Psi(\bar{r} + N_3\bar{c}) = \Psi(\bar{r})$$

For a Bloch state, the above conditions mean that

$$e^{-i\bar{k} \cdot N_1\bar{a}} = e^{-i\bar{k} \cdot N_2\bar{b}} = e^{-i\bar{k} \cdot N_3\bar{c}}$$

This condition can be satisfied only if

$$\bar{k} = \frac{2\pi m_1}{N_1} \bar{a}^* + \frac{2\pi m_2}{N_2} \bar{b}^* + \frac{2\pi m_3}{N_3} \bar{c}^*$$

where

$m_1, m_2,$ and m_3 are integers
 a^*, b^*, c^* are the reciprocal lattice vectors

The allowed values of $m_1, m_2,$ and m_3 must run through the values:

$$0 \leq m_1 \leq N_1, \quad 0 \leq m_2 \leq N_2, \quad \text{and} \quad 0 \leq m_3 \leq N_3$$

However, this is not the proper range, and the appropriate extent is

$$-\frac{N_1}{2} \leq m_1 \leq \frac{N_1}{2}, \quad -\frac{N_2}{2} \leq m_2 \leq \frac{N_2}{2}, \quad \text{and} \quad -\frac{N_3}{2} \leq m_3 \leq \frac{N_3}{2}$$

which will give a cell centered in origin, as was previously observed for the Wigner–Seitz in real space, but now in the \bar{k} space. This cell is named the Brillouin zone, which is the Wigner–Seitz cell in the \bar{k} space or inverse space.

The number of allowed states is then $N_1 \times N_2 \times N_3 = M$, which is the number of cells in a real macroscopic finite crystal. That is, the number of allowed wave vectors in a Brillouin zone is exactly the number of unit cells in the crystal under consideration.

1.4 LATTICE VIBRATIONS

1.4.1 PHONONS

Lattice vibrations are fundamental for the understanding of several phenomena in solids, such as heat capacity, heat conduction, thermal expansion, and the Debye–Waller factor. To mathematically deal with lattice vibrations, the following procedure will be undertaken [7]: the solid will be considered as a crystal lattice of atoms, behaving as a system of coupled harmonic oscillators. Thereafter, the normal oscillations of this system can be found, where the normal modes behave as uncoupled harmonic oscillators, and the number of normal vibration modes will be equal to the degrees of freedom of the crystal, that is, $3nM$, where n is the number of atoms in the unit cell and M is the number of units cell in the crystal [8].

In order to solve this problem, it is possible to use the Hamiltonian procedure of classical mechanics [8]. Hence, the classical Hamiltonian of a system of coupled harmonic oscillators can be written as follows [7]:

$$H = \sum_i \frac{(p'_i)^2}{2m_i} + \sum_{i,j} \frac{1}{2} C'_{i,j} q'_i q'_j \quad (1.10)$$

where

q'_i are the coordinates of displacement from the equilibrium position

$p'_i = m_i \frac{dq'_i}{dt}$ are the impulses

$C'_{i,j} = C'_{j,i}$ are constants

The Hamiltonian can be simplified if we made the following substitutions in order to eliminate the constant

$$q_i = q'_i \sqrt{m_i}$$

and

$$C_{i,j} = \frac{C'_{i,j}}{\sqrt{m_i m_j}}$$

And finally,

$$p_i = \frac{\partial L}{\partial \dot{q}_i} = \frac{p'_i}{\sqrt{m_i}}$$

where L is the Lagrangian function. Consequently, the Hamiltonian can be written as follows:

$$H = \sum_i \frac{(p_i)^2}{2} + \sum_{i,j} \frac{1}{2} C_{i,j} q_i q_j \quad (1.11)$$

Following the rules of the Hamiltonian method, the equations of motion can be written as follows:

$$\dot{p}_i = -\frac{\partial H}{\partial q_i} = -\sum_j C_{i,j} q_j \quad \text{and} \quad \dot{q}_i = \frac{\partial H}{\partial p_i} = p_i \quad (1.12)$$

Equation 1.12 is a system of linear differential equations with constant coefficients. Then, following the rules for solving this type of an equation, its solution can be written in the following form [7]:

$$q_i^\beta = e^{-i\omega_\beta t} c_i^\beta$$

where

$\omega_\beta = 2\pi \nu_\beta$ are the angular frequencies

ν_β are frequencies

The condition for solving this system is [9]

$$|C_{i,j} - \omega^2 \delta_{i,j}| = 0 \quad (1.13)$$

which gives an equation that allows us to get the values of ω_β and the corresponding orthogonal vectors c_i^β

$$\sum_i c_i^\beta c_i^\delta = \delta_{\beta\delta}$$

where the general solution for q_i has the following form:

$$q_i = \sum_\beta L_\beta q_i^\beta \quad (1.14)$$

where L_β are constants. In essence, during the previous procedure we have separated the motion of the system in normal vibration modes, where each one has a frequency ω_β . Thereafter, the motion of the system is described as a sum of normal vibration modes.

Now making the following substitution [7]

$$Q_{\beta} = L_{\beta} e^{-i\omega_{\beta} t}$$

it is then possible to make the following variable substitution:

$$q_i = \sum_{\beta} Q_{\beta} c_i^{\beta}$$

And then get [10]

$$H = \sum_i h_{\beta} \quad (1.15)$$

where

$$h_{\beta} = \frac{1}{2} p_{\beta}^2 + \frac{1}{2} \omega_{\beta}^2 Q_{\beta}^2 \quad (1.16)$$

If we now change the coordinates and the momentum by their quantum mechanical corresponding operators, we will get

$$\hat{H} = \sum_i \hat{h}_{\beta}$$

in which

$$\hat{h}_{\beta} = -\frac{\hbar^2}{2} \frac{\partial^2}{\partial Q_{\beta}^2} + \frac{1}{2} \omega_{\beta}^2 Q_{\beta}^2$$

where

$$\hbar = \frac{h}{2\pi}$$

and h is the Planck's constant. This is the Schrödinger equation for a quantum harmonic oscillator of frequency ω_{β} . Therefore, the energy of the system will be

$$E = \sum_{\beta} \left(N_{\beta} + \frac{1}{2} \right) \hbar \omega_{\beta} \quad (1.17)$$

where

$$E_n = \left(n + \frac{1}{2} \right) \hbar \omega \quad (1.18)$$

are the energy levels of a quantum harmonic oscillator. Consequently, we have reduced the lattice energy to the summation of the energy of different noncoupled harmonic oscillators.

It is very well known that Einstein, developing Planck's ideas, quantized the electromagnetic field by introducing a quantum particle named the photon. Consequently, each mode or state of a classical electromagnetic field is characterized by an angular frequency, ω , and a wave vector, $\vec{k} = \frac{2\pi}{\lambda} \vec{s}$, in which \vec{s} is a unit vector normal to the wave fronts. Then, the modes or states are replaced by the photon that carries energy

$$E = \hbar\omega$$

and momentum

$$\vec{p} = \hbar\vec{k}$$

where

$$\hbar = \frac{h}{2\pi}$$

$\omega = 2\pi\nu$ is the angular frequency

ν is the frequency of the electromagnetic radiation

λ is the wavelength of the electromagnetic radiation

Similarly, during their effort to understand the thermal energy of solids, Einstein and Debye quantized the lattice waves and the resulting quantum was named phonon. Consequently, it is possible to consider the lattice waves as a gas of noninteracting quasiparticles named phonons, which carries energy, $E = \hbar\omega$, and momentum, $\vec{p} = \hbar\vec{k}$. That is, each normal mode of oscillation, which is a one-dimensional harmonic oscillator, can be considered as a one-phonon state.

1.4.2 BOSE-EINSTEIN DISTRIBUTION

It is possible to calculate the average energy for a single oscillation mode, following the canonical ensemble methodology [6,11] as

$$\langle E \rangle = \frac{\sum_0^{\infty} \left(n + \frac{1}{2}\right) \hbar\omega e^{-\frac{\left(n + \frac{1}{2}\right) \hbar\omega}{kT}}}{\sum_0^{\infty} e^{-\frac{\left(n + \frac{1}{2}\right) \hbar\omega}{kT}}} = \frac{\hbar\omega}{2} + \frac{\sum_0^{\infty} n \hbar\omega e^{-\frac{\left(n + \frac{1}{2}\right) \hbar\omega}{kT}}}{\sum_0^{\infty} e^{-\frac{\left(n + \frac{1}{2}\right) \hbar\omega}{kT}}}$$

where k is the Boltzmann constant. It is easy to show that

$$\langle E \rangle = \frac{\hbar\omega}{2} - \frac{\partial}{\partial \left(\frac{1}{kT}\right)} \ln \left(\sum_0^{\infty} e^{-\frac{\hbar\omega}{kT}} \right) = \left(\frac{e^{-\frac{\hbar\omega}{kT}}}{1 - e^{-\frac{\hbar\omega}{kT}}} + \frac{1}{2} \right) \hbar\omega = \left(n(\omega, T) + \frac{1}{2} \right) \hbar\omega$$

Consequently,

$$n(\omega, T) = \frac{1}{e^{\frac{\hbar\omega}{kT}} - 1} \quad (1.19)$$

which is the Bose–Einstein distribution function. Consequently, phonons behave as bosons [12]. If we use Equation 1.19 to describe each vibration mode, then

$$n_{\beta}(\omega_{\beta}, T) = \frac{1}{e^{\frac{\hbar\omega_{\beta}}{kT}} - 1} \quad (1.20)$$

Then, Equation 1.20 tells us that there are on average $n_{\beta}(\omega_{\beta}, T)$ phonons in the β mode, where this mode contributes energy

$$\langle E_{\beta} \rangle = \left(n_{\beta}(\omega_{\beta}, T) + \frac{1}{2} \right) \hbar\omega_{\beta}$$

1.4.3 HEAT CAPACITY OF SOLIDS

The average energy in the canonical ensemble of the whole system is

$$U = \langle E_T \rangle = E_0 + \sum_{\beta} \hbar\omega_{\beta} \left(\frac{1}{e^{\frac{\hbar\omega_{\beta}}{kT}} - 1} \right) \quad (1.21)$$

Besides, the canonical partition function [11] of the system of oscillators is [13]

$$Z = e^{-\frac{E_0}{kT}} \prod_{\beta} \frac{1}{1 - e^{-\frac{\hbar\omega_{\beta}}{kT}}}$$

Then,

$$\ln Z = \frac{E_0}{kT} - \sum_{\beta} \ln \left(1 - e^{-\frac{\hbar\omega_{\beta}}{kT}} \right) \quad (1.22)$$

We will now attempt an analysis of Equation 1.21 for n mol of a metallic, ionic, or covalent crystal, with 1 ion per lattice site, that is, for an Avogadro number, N_A , of ions at a high temperature. At these conditions, $kT \gg \hbar\omega_{\beta}$, and, consequently,

$$\langle E_T \rangle = E_0 + \sum_{\beta} \hbar\omega_{\beta} \left(\frac{1}{e^{\frac{\hbar\omega_{\beta}}{kT}} - 1} \right) = E_0 + \sum_{\alpha} kT = E_0 + 3NkT = E_0 + 3nRT \quad (1.23)$$

where n is the number of moles.

Since the heat capacity at constant volume is defined as

$$C_V = \left(\frac{\partial U}{\partial T} \right)_V = \left(\frac{\partial \langle E_T \rangle}{\partial T} \right)_V \quad (1.24)$$

then with the help of Equations 1.23 and 1.24, we can obtain, for $n = 1$

$$C_V = 3R$$

which is the Dulong–Petit law, where $R = kN_A$ is the ideal gas constant. The same result can as well be obtained with the following argument: a classical harmonic oscillator included in a system of harmonic oscillators (as is the proposed model of a solid) in thermal equilibrium at a temperature T has an average energy equal to kT , since the number of normal modes is $3N$, where $N = nN_A$ is the number of atoms in the solid, N_A is the Avogadro number, and n , the number of moles. Then, the average classical internal energy of a solid for $n = 1$ is $3RT$ and $C_V = 3R$.

However, we need to know the behavior of solids at all temperatures. Einstein, in 1907, to deal with the problem, assumed that all the normal vibration modes have the same angular frequency ω_E . As a result, Equation 1.21 will take the following form [12]:

$$\langle E_T \rangle = E_0 + \frac{3N_A \hbar \omega_E}{e^{\frac{\hbar \omega_E}{kT}} - 1} = E_0 + \frac{3N_A k \Theta_E}{e^{\frac{\Theta_E}{T}} - 1}$$

where

$$k\Theta_E = \hbar\omega_E$$

Θ_E is a characteristic temperature of the system

Consequently, the heat capacity at a constant volume will be

$$C_V = 3N_A k \left(\frac{\Theta_E}{T} \right)^2 \frac{e^{\frac{\Theta_E}{T}}}{\left(e^{\frac{\Theta_E}{T}} - 1 \right)^2}$$

where the limit for the high temperature is $C_V = 3R$

Debye, in 1912, made more realistic assumptions in order to deal with the lattice vibration problem. He considered that because of the large number of atoms in the crystal the number of normal vibration modes is very high, and it is possible to consider that the vibrations are continuously distributed over a specified range of frequencies, $0 < \nu < \nu_m$, where the distribution is such that the number of normal vibration modes in the interval from ν to $\nu + d\nu$ is $g(\nu)d\nu$. Consequently, in Equation 1.22, it is possible to substitute the summation for the integration. Therefore [13],

$$\ln Z = -\frac{E_0}{kT} - \int_0^{\nu_m} \ln \left(1 - e^{-\frac{\hbar \nu \alpha}{kT}} \right) g(\nu) d\nu \quad (1.25)$$

The density of elastic standing waves in a continuous solid is given by [14]

$$g(\nu) = \frac{12\pi V \nu^2}{V_s^3} \quad (1.26a)$$

where

- V_s is the average speed of sound waves in the solid
- ν is the frequency of the standing wave
- V is the volume of the solid

The derivation of Equation 1.26a is carried out by calculating the number of standing waves in a cubic cavity of volume V , and follows a process similar to that applied in Section 1.5.3 for calculating the density of states for an electron gas [14].

Now, since

$$\int_0^{\nu_m} g(\nu) d\nu = \int_0^{\nu_m} \frac{12\pi\nu^2}{V_s^3} d\nu = 3N_A$$

then

$$\nu_m = \left(\frac{3N_A V_s^3}{4\pi V} \right)^{\frac{1}{3}}$$

and

$$g(\nu) = \frac{9N_A}{\nu_m^3} \nu^2 \quad (1.26b)$$

Substituting Equation 1.26 in Equation 1.25, we will get

$$\ln Z = -\frac{E_0}{kT} - \frac{9N_A}{\nu_m^3} \int_0^{\omega_m} \nu^2 \ln \left(1 - e^{-\frac{h\nu}{kT}} \right) d\nu$$

Then, using [11]

$$U = kT^2 \left(\frac{\partial \ln Z}{\partial V} \right) \quad \text{and} \quad C_V = \left(\frac{\partial U}{\partial T} \right)_V = \left(\frac{\partial \langle E_T \rangle}{\partial T} \right)_V$$

we will get (Figure 1.8).

$$C_V = 9N_A k \left(\frac{T}{\Theta_D} \right) \int_0^{\frac{\Theta_D}{T}} \frac{y^4 e^y}{e^y - 1} dy \quad (1.27)$$

where

- $k\Theta_D = h\nu_m$ defines the Debye temperature, Θ_D
- $y = \frac{h\nu}{kT}$ is an integration variable

The integral in Equation 1.27 cannot be analytically solved; however, for a high temperature,

$$\frac{T}{\Theta_D} \gg 1,$$

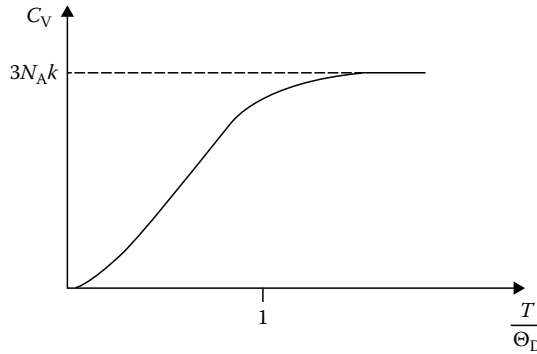


FIGURE 1.8 Graphic representation of the Debye law of specific heat.

$$C_V = 9N_A k \left(\frac{T}{\Theta_D} \right) \int_0^{\frac{\Theta_D}{T}} y^4 dy = 9N_A k \left(\frac{T}{\Theta_D} \right)^3 \left(\frac{1}{3} \right) \left(\frac{\Theta_D}{T} \right)^3 = 3N_A k$$

On the other hand, the integral in Equation 1.27 for a low temperature, $\frac{T}{\Theta_D} \ll 1$, can be written as follows:

$$C_V = 9N_A k \left(\frac{T}{\Theta_D} \right) \int_0^{\frac{\Theta_D}{T}} \frac{y^4 e^y}{e^y - 1} dy \approx 9N_A k \left(\frac{T}{\Theta_D} \right) \int_0^{\infty} \frac{y^4 e^y}{e^y - 1} dy \quad (1.28)$$

Then, the integral in the right of Equation 1.28 can be integrated as follows:

$$C_V = \frac{12\pi^4}{5} N_A k \left(\frac{T}{\Theta_D} \right)^3$$

1.5 ELECTRONS IN CRYSTALLINE SOLID MATERIALS

1.5.1 ELECTRON GAS

In a free atom of a metallic element, the valence electron moves in an orbital around the ion formed by the nucleus and the core electrons. When a solid metal is formed, these external orbitals overlap and interact. Subsequently, the outer electrons do not belong anymore to the atom. In this case, the wave function describing the state of these electrons is a solution of the Schrödinger equation for the motion in the potential of all the ions. As a consequence, in a metal, the bonding is carried out by the conduction electrons that form a cloud of electrons, which fills the space between the metal ions and mutually joins the ions throughout the Coulombic attraction between the electron gas and positive metal ions [14–16]. In this regard, the metallic crystal is held together by electrostatic forces of attraction between the positively charged metal ions and the nonlocalized, negatively charged electrons, that is, the electron gas. In the framework of the electron gas model or the Drude model, the system is formed by the cations plus a free electron gas. The premises behind the Drude model are [14–16]

- Electrons collide with positive ions.
- Collisions are instantaneous events.
- Electrons lose all extra energy gained from the external electric field during a collision.
- Between collisions the electrons moves freely.
- Mutual repulsion between electrons is ignored.
- Finally, it is possible to state that the electron is confined to an energy band, named the conduction band, as will be explained later.

Now, if free electrons are influenced by an external electric field, \bar{E}_x , then a net electron drift in the x -direction is produced (see Figure 1.9). This net drift, along the force, which is created by the electric field, is superimposed on the chaotic motion of the electron gas. The end result of this process is that, following numerous scattering episodes, the electron has moved by a net distance, Δx , from its initial position in the direction of the positive terminal.

Following these assumptions, the Newton motion equation, along the x -axis, for the electrons in the free electron gas is given by

$$m_e \frac{dv_x}{dt} = e E_x - m_e \frac{v_x}{\tau}$$

where

τ is the time between collisions

m_e and e are the mass and charge of the electron

Then, the steady-state solution of the Newton equation for the electron in the electron gas under the influence of an external electric field is given by

$$v_x^{\text{drift}} = \frac{e\tau}{m_e} E_x$$

Now,

$$J_x = \sigma E_x$$

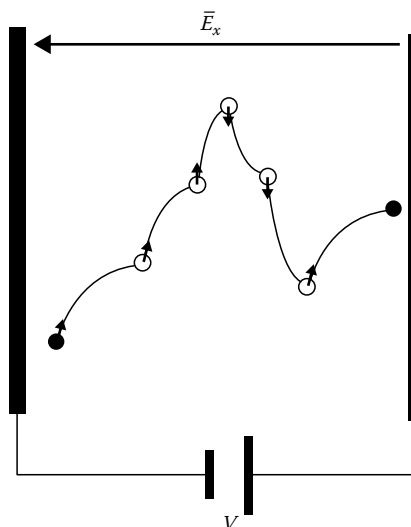


FIGURE 1.9 Electron trajectories in the electron gas or Drude model.

where

J_x is the current density
 σ is the conductivity

And with the help of the definition of mobility, M ,

$$v_x^{\text{drift}} = ME_x$$

It is possible to show that

$$\sigma = \frac{ne^2\tau}{m_e} = neM \quad (1.29)$$

The previously described theory in its original form assumes that the classical kinetic theory of gases is applicable to the electron gas, that is, electrons are expected to have velocities that are temperature dependent according to the Maxwell–Boltzmann distribution law. But, the Maxwell–Boltzmann energy distribution has no restrictions to the number of species allowed to have exactly the same energy. However, in the case of electrons, there are restrictions to the number of electrons with identical energy, that is, the Pauli exclusion principle; consequently, we have to apply a different form of statistics, the Fermi–Dirac statistics.

1.5.2 FERMI–DIRAC DISTRIBUTION

One of the simplest procedures to get the expression for the Fermi–Dirac (F–D) and the Bose–Einstein (B–E) distributions, is to apply the grand canonical ensemble methodology for a system of noninteracting indistinguishable particles, that is, fermions for the Fermi–Dirac distribution and bosons for the Bose–Einstein distribution. For these systems, the grand canonical partition function can be expressed as follows [12]:

$$\Theta = \sum_{N=0}^{\infty} \lambda^N \sum_{\{N_k\}} e^{-\frac{\sum_k N_k \varepsilon_k}{kT}} \quad (1.30)$$

where

ε_k are the energy states of the individual particles is the number of particles in the system

$\lambda = e^{-\frac{\mu}{kT}}$, in which μ is the chemical potential of the system of N indistinguishable noninteracting particles

The summation over $\{N_k\}$ means that we are summing the particle distributions in the energy states accessible to the system where

$$N = \sum_k N_k$$

and

$$E_j = \sum_k N_k \varepsilon_k$$

is the energy of the particle system; then, rearranging Equation 1.30 leads to

$$\Theta = \sum_{N=0}^{\infty} \lambda^N \sum_{\{N_k\}} e^{-\frac{\sum_k N_k \epsilon_k}{kT}} = \sum_{N=0}^{\infty} \sum_{\{N_k\}} \lambda^{\sum_i N_i} e^{-\frac{\sum_k N_k \epsilon_k}{kT}} = \sum_{N=0}^{\infty} \sum_{\{N_k\}} \prod_k \left(\lambda e^{-\frac{\epsilon_k}{kT}} \right)^{N_k} \quad (1.31)$$

And continuing with the rearrangement of Equation 1.31, we will get

$$\Theta = \sum_{N_1=0}^{N_1^{\max}} \sum_{N_2=0}^{N_2^{\max}} \cdots \prod_k \left(\lambda e^{-\frac{\epsilon_k}{kT}} \right)^{N_k} = \sum_{N_1=0}^{N_1^{\max}} \lambda e^{-\frac{\epsilon_1}{kT}} \sum_{N_2=0}^{N_2^{\max}} \lambda e^{-\frac{\epsilon_2}{kT}} \cdots = \prod_k \sum_{N_k=0}^{N_k^{\max}} \left(\lambda e^{-\frac{\epsilon_k}{kT}} \right)^{N_k} \quad (1.32)$$

We know from the Pauli principle that for fermions $N_k = 0$ and $N_k = 1$. Consequently,

$$\Theta = \prod_k \left(1 + \lambda e^{-\frac{\epsilon_k}{kT}} \right)^{N_k} = \prod_k \left(1 + e^{-\frac{\epsilon_k - \mu}{kT}} \right)^{N_k}$$

Since [11,12]

$$\bar{N} = kT \left(\frac{\partial \ln \Theta(V, T, \mu)}{\partial \mu} \right)_{V, T} = \sum_k \frac{\lambda e^{-\frac{\epsilon_k}{kT}}}{1 + \lambda e^{-\frac{\epsilon_k}{kT}}} \quad (1.33)$$

the average number of particles in the state k in the Fermi–Dirac distribution is

$$\bar{N}_k = \frac{\lambda e^{-\frac{\epsilon_k}{kT}}}{1 + \lambda e^{-\frac{\epsilon_k}{kT}}} \quad (1.34)$$

As a corollary, in the case of bosons, since $N_k = 0, 1, 2, 3, \dots, \infty$, then

$$\bar{N}_k = \frac{\lambda e^{-\frac{\epsilon_k}{kT}}}{1 - \lambda e^{-\frac{\epsilon_k}{kT}}} \quad (1.35)$$

which is equivalent to the previously obtained Bose–Einstein distribution, since in the case of bosons, there is no restriction on the total number of particles, and $\mu = 0$ [17].

In this regard, the probability of finding an electron in a state with energy E is given by the Fermi–Dirac distribution function, $f(E)$, which is expressed as follows (Figure 1.10):

$$f_{\text{FD}}(E) = \frac{1}{e^{\frac{E-\mu}{kT}} + 1} = \frac{1}{e^{\frac{E-E_F}{kT}} + 1}$$

where

E is the state energy

$\mu = E_F$ is the Fermi energy level

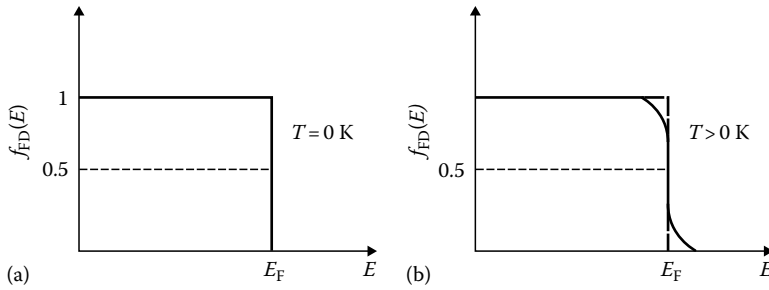


FIGURE 1.10 (a) Fermi–Dirac distribution for $T = 0$ K and (b) Fermi–Dirac distribution for $T > 0$ K.

k is the Boltzmann constant
 T is the absolute temperature

The Fermi–Dirac distribution describes the statistics of electrons in the conduction band of a solid when the electrons interact with each other and the environment, so that they obey the Pauli exclusion principle.

In Figure 1.10, it is shown that the Fermi level is the energy of the highest occupied quantum state in a system of fermions at 0 K, and that above 0 K, because of thermal excitation, some of the electrons are at energies above E_F .

1.5.3 DENSITY OF STATES FOR THE ELECTRON GAS

We will now calculate the density of electron states in the case of the electron gas. In this model, the core electrons are considered as nearly localized, and must be distinguished from the conduction electrons, which are supposed to freely move in Bloch states throughout the whole crystal [5]. Because of the fact that the potential is constant, the single-particle Hamiltonian is merely the kinetic energy of the electron, that is,

$$\hat{H} = -\frac{\hbar^2}{2m} \nabla^2 \quad (1.36)$$

Then, the conduction electron states are plane waves, that is,

$$\Psi_{\vec{k}} = e^{i\vec{k} \cdot \vec{r}} \quad (1.37)$$

But, the real wave function must include the spin coordinate, then [6]

$$\Psi_{\vec{k},s} = e^{i\vec{k} \cdot \vec{r}} \chi(s) \quad (1.38)$$

where

$$\chi\left(\frac{1}{2}\right) = \begin{pmatrix} 1 \\ 0 \end{pmatrix}$$

and

$$\chi\left(-\frac{1}{2}\right) = \begin{pmatrix} 0 \\ 1 \end{pmatrix}$$

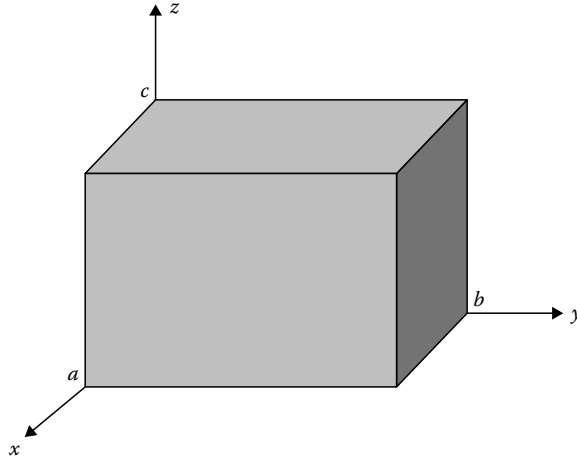


FIGURE 1.11 Box of volume $V = abc$ where the electrons are confined.

Substituting Equation 1.38 in Equation 1.36, we will get the energy of the electrons that is independent of the spin state [12,15]

$$E^0(k) = \frac{\hbar^2 k^2}{2m_e} \quad (1.39)$$

where $k = |\vec{k}|$. Then, the system in consideration is equivalent to a quantum system of noninteracting electrons in the three-dimensional potential box (see Figure 1.11) [11,17]. In this case, the possible energies for electrons confined in a cubic box of volume, $V = abc$, are given by

$$E(n_1, n_2, n_3) = \frac{h^2}{8m_e} \left(\frac{n_1^2}{a^2} + \frac{n_2^2}{b^2} + \frac{n_3^2}{c^2} \right)$$

where n_1 , n_2 , and n_3 are quantum numbers, each of which can be any integer number except 0. For a square box, where $a = b = c = L$, we will have

$$E(n_1, n_2, n_3) = \frac{h^2}{8L^2 m_e} (n_1^2 + n_2^2 + n_3^2) = \frac{h^2 R^2}{8m_e L^2} \quad (1.40)$$

where we have defined the sphere of radius

$$R^2 = (n_1^2 + n_2^2 + n_3^2) = \frac{E}{A}$$

in which

$$A = \frac{h^2}{8L^2 m_e}$$

Consequently, the number of states that can be accommodated in the space defined by $\vec{n} = n_1 \vec{i} + n_2 \vec{j} + n_3 \vec{k}$ (see Figure 1.12) is

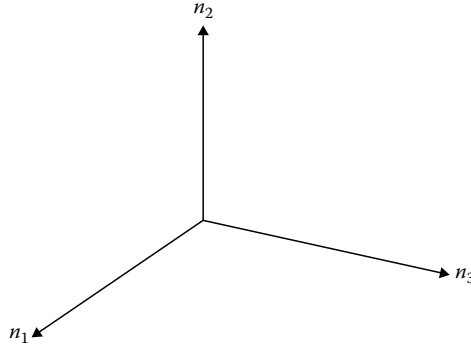


FIGURE 1.12 $\vec{n} = n_1\vec{i} + n_2\vec{j} + n_3\vec{k}$, space.

$$\eta = 2 \left(\frac{1}{8} \right) \left(\frac{4}{3} \pi R^3 \right) = \frac{1}{3} \pi \left(\frac{E}{A} \right)^{\frac{3}{2}} \quad (1.41)$$

where the factor 2 is due to the two spin states and the factor 1/8 is because only positive numbers of the quantum states are allowed. Then the density of states can be defined as follows:

$$g(E) = \frac{d\eta}{dE} = \frac{\pi}{2} \left(\frac{\sqrt{E}}{A^{3/2}} \right) \quad (1.42)$$

In this regard, if the probability of occupancy of a state at an energy E is $f_{\text{FD}}(E)$, in agreement with the Fermi–Dirac distribution, we are dealing with electrons, which are fermions. Then, the product $f_{\text{FD}}(E)g(E)$ is the number of electrons per unit energy per unit volume. Consequently, the area under the curve with the energy axis gives

$$N = \int_0^{\infty} g(E)f_{\text{FD}}(E)dE \quad (1.43)$$

which is the number of free electrons in volume V .

We can now calculate the value of the Fermi energy level, because as the electrons fulfill the Pauli exclusion principle, only two electrons can occupy one energy state thereafter, since at $T = 0$ [K], $f_{\text{FD}}(E) = 1$, for $E < E_{\text{F}}(0)$ and $f_{\text{FD}}(E) = 0$; for $E > E_{\text{F}}(0)$, then

$$N = \int_0^{E_{\text{F}}(0)} g(E) dE = \frac{\pi}{2A^{3/2}} \int_0^{E_{\text{F}}(0)} \sqrt{E} dE = \frac{\pi}{3A^{3/2}} [E_{\text{F}}(0)]^{3/2}$$

And as a result

$$E_{\text{F}}(0) = \frac{\hbar^2}{8m_e} \left(\frac{3N}{\pi L^3} \right)^{2/3} = \frac{\hbar^2}{8m_e} \left(\frac{3n}{\pi} \right)^{2/3} \quad (1.44)$$

where $n = \left(\frac{N}{V} \right)$ and $V = L^3$

It is easy now to calculate the mean energy of an electron in a solid, $\bar{\epsilon}_{\text{average}}$, at $T = 0$ [K], as follows:

$$\bar{\epsilon}_{\text{average}}(0) = \frac{1}{N} \int_0^{\infty} E g(E) f_{\text{FD}}(E) dE = \frac{1}{N} \int_0^{E_{\text{F}}(0)} E g(E) dE = \left(\frac{3}{5}\right) E_{\text{F}}(0)$$

Above absolute zero, the average energy is approximately [2,15]

$$\bar{\epsilon}_{\text{average}}(T) = \left(\frac{3}{5}\right) E_{\text{F}}(0) \left[1 + \frac{5\pi^2}{12} \left(\frac{kT}{E_{\text{F}}(0)} \right)^2 \right]$$

Since $E_{\text{F}}(0) \gg kT$

$$\bar{\epsilon}_{\text{average}}(T) \approx \bar{\epsilon}_{\text{average}}(0) = \frac{1}{2} m (\bar{v}_{\text{F}})^2$$

where \bar{v}_{F} is the root mean-square speed of the electrons in the valence band of a solid around the Fermi level. Then

$$\bar{v}_{\text{F}} = \left(\frac{6E_{\text{F}}(0)}{5m} \right)^{1/2} \quad (1.45)$$

This velocity of the electron is independent of temperature, in contradiction to the Maxwell-Boltzmann statistic, which states that

$$\left(\frac{1}{2} \right) m \langle v_e^2 \rangle = \frac{3}{2} kT$$

1.5.4 ENERGY BAND MODEL

The electron gas model adequately describes the conduction of electrons in metals; however, it has a problem, that is, the electrons with energy near the Fermi level have wavelength values comparable to the lattice parameters of the crystal. Consequently, strong diffraction effects must be present (see below the diffraction condition (Equation 1.47)). A more realistic description of the state of the electrons inside solids is necessary. This more accurate description is carried out with the help of the Bloch and Wilson band model [18].

If the problem is mathematically treated as a perturbation of the free-electron gas energy states caused by the presence of the periodic potential, $V(\vec{r})$, in the Schrödinger equation, then

$$-\frac{\hbar^2}{2m} \nabla^2 \psi(\vec{r}) + V(\vec{r}) \psi(\vec{r}) = E \psi(\vec{r})$$

Then [5],

$$E(\vec{k}) = E^0(k) + \int \psi_{\vec{k}}(\vec{r}) V(\vec{r}) \psi_{\vec{k}}(\vec{r}) d^3\vec{r} + \sum_{\vec{k}'} \frac{\int \psi_{\vec{k}}(\vec{r}) V(\vec{r}) \psi_{\vec{k}'}(\vec{r}) d^3\vec{r}}{E^0(\vec{k}) - E^0(\vec{k}')} \quad (1.46)$$

where

$$E^0(k) = \frac{\hbar^2 k^2}{2m}$$

Since diffraction is an effect linked to scattering, if a beam of fast electrons is being directed into a crystal, its scattering process will be described by the Born approximation where the rate of transition between the initial state, $\Psi_{\bar{k}}$, and the final state, $\Psi_{\bar{k}'}$, is given by [10]

$$P_{\bar{k},\bar{k}'} = \int \Psi_{\bar{k}} V(\vec{r}) \Psi_{\bar{k}'} d^3\vec{r}$$

Given that [5,6]

$$V(\vec{r}) = \sum_{\vec{G}_{hkl}} V_{\vec{G}_{hkl}} e^{i\vec{G}_{hkl} \cdot \vec{r}}$$

and

$$\Psi_{\bar{k}} = e^{i\bar{k} \cdot \vec{r}}$$

then

$$P_{\bar{k},\bar{k}'} = \sum_{\vec{G}_{hkl}} \int e^{i(\bar{k} + \vec{G}_{hkl} - \bar{k}') \cdot \vec{r}} d^3\vec{r}$$

where

$$P_{\bar{k},\bar{k}'} = V_{\vec{G}_{hkl}}$$

If the diffraction condition for electrons in a crystal (Equation 1.47)

$$\bar{k} - \bar{k}' = \vec{G}_{hkl} \quad (1.47)$$

is fulfilled, then

$$P_{\bar{k},\bar{k}'} = 0$$

Subsequently, introducing the diffraction condition in Equation 1.46, we will get [5]

$$E(\bar{k}) = \frac{\hbar^2 k^2}{2m} + V_0 + \sum_{\vec{G}_{hkl} \neq 0} \frac{|V_{\vec{G}_{hkl}}|^2}{E^0(\bar{k}) - E^0(\bar{k}' - \vec{G}_{hkl})}$$

Consequently, the periodicity condition of the potential produces the segmentation in the energy bands.

A more exact treatment is made using the Bloch theorem. In this sense, the solution of the Schrödinger equation may be a plane wave multiplied by a periodic function, that is,

$$\Psi_{\vec{k}}^-(\vec{r}) = e^{-i\vec{k}\cdot\vec{r}} u_{\vec{k}}^-(\vec{r})$$

where

$$u_{\vec{k}}^-(\vec{r}) = \sum_{\vec{G}_{hkl}} u_{\vec{G}_{hkl}}^-(\vec{k}) e^{i\vec{G}_{hkl}\cdot\vec{r}} \quad (1.48)$$

Due to the periodicity of $u_{\vec{k}}^-(\vec{r})$, if we insert Equation 1.48 in the Schrödinger equation [6]

$$\left(-\frac{\hbar^2}{2m} \nabla^2 + \sum_{\vec{G}'_{hkl}} V_{\vec{G}'_{hkl}} e^{i\vec{G}'_{hkl}\cdot\vec{r}} - E \right) \sum_{\vec{G}_{hkl}} u_{\vec{G}_{hkl}}^- e^{i\vec{G}_{hkl}\cdot\vec{r}} = 0$$

Then

$$\left(\frac{\hbar^2}{2m} (\vec{k} + \vec{G})^2 - E \right) u_{\vec{G}_{hkl}}^-(\vec{k}) + \sum_{\vec{G}'_{hkl}} V_{\vec{G}'_{hkl}} u_{\vec{G}'_{hkl} - \vec{G}_{hkl}}^- = 0 \quad (1.49)$$

This equation is named the Bloch difference equation and is a set of coupled linear equations whose nontrivial solution conditions are

$$\left| \left(\frac{\hbar^2}{2m} (\vec{k} + \vec{G})^2 - E \right) \delta_{\vec{G}_{hkl}, \vec{G}'_{hkl}} + V_{\vec{G}'_{hkl} - \vec{G}_{hkl}} \right| = 0 \quad (1.50)$$

This is named the Hill determinant. After solving, the resulting secular determinant for the root of $E_n(\vec{k})$ provides a more accurate method for calculating the band structure of solids, where $n = 1$ refers to the first band, $n = 2$ to the second, and so on.

1.5.5 MOLECULAR ORBITAL APPROACH FOR THE FORMATION OF ENERGY BANDS

A crystalline solid can be considered as a huge, single molecule; subsequently, the electronic wave functions of this giant molecule can be constructed with the help of the molecular orbital (MO) methodology [19]. That is, the electrons are introduced into crystal orbitals, which are extended along the entire crystal, where each crystal orbital can accommodate two electrons with opposite spins. A good approximation for the construction of a crystal MO is the linear combination of atomic orbitals (LCAO) method, where the MOs are constructed as a LCAO of the atoms composing the crystal [19].

For example, in metals, because of their large electrical conductivity, it seems that at least some of the electrons can move freely through the bulk of the metal, while the core electrons remain in their atomic orbital, similar to the isolated atoms forming the metal. For example, let us take into account the formation of a linear array of lithium atoms from individual lithium atoms: Li–Li; Li–Li–Li; Li–Li–Li–Li.... Then, the first stage is the formation of a lithium molecule, Li_2 . This molecule is analogous to the hydrogen molecule, H_2 [15,19]. In the formation of the H_2 molecule, two MOs are formed, that is, the bonding MO

$$\Psi_{\sigma} = \psi_{1s}(\vec{r}_A) + \psi_{1s}(\vec{r}_B)$$

and the antibonding MO

$$\Psi_{\sigma^*} = \psi_{1s}(\vec{r}_A) - \psi_{1s}(\vec{r}_B)$$

where the two electrons pair their spins and occupy the bonding orbital. Then the two lithium atoms are bound together by a pair of valence electrons, where each lithium atom supplies its 2s electron to form a covalent molecular bond (see Figure 1.13). In this case, the molecule formed occurs in lithium vapor.

We will now take into account the hypothetical linear molecule, Li_3 . The valence electron cloud is spherical; then, in the course of the linear combination of atomic orbitals, the three atomic valence electron clouds overlap to form one continuous distribution, and two distributions with nodes, that is, three MOs (see Figure 1.14). While the length of the chain is augmented, the number of electronic states, into which the atomic 2s state splits during the linear combination of atomic orbitals, increases. In this regard, the number of states equals the number of atoms.

A similar situation takes place when lithium chains are placed side by side or stacked on top of each other, so that finally the space lattice of the lithium crystal is obtained. In this case, the electronic states have energies that are bounded by an upper and lower limiting value, forming an energy band of closely spaced values (see Figure 1.14). Similarly, energy bands can also result from overlapping p and d orbitals.

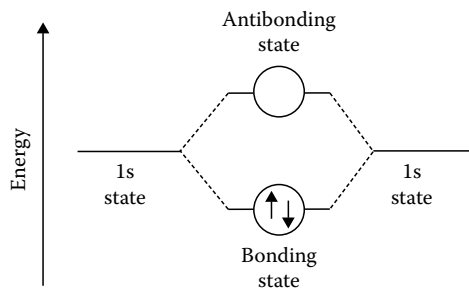


FIGURE 1.13 Energy of the states formed during the establishment of a Li_2 molecule.

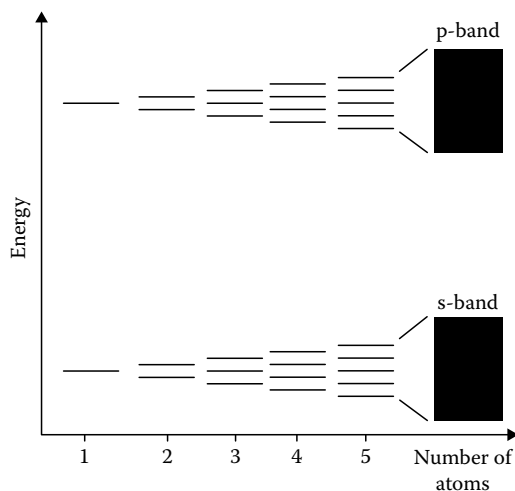


FIGURE 1.14 Band formation process.

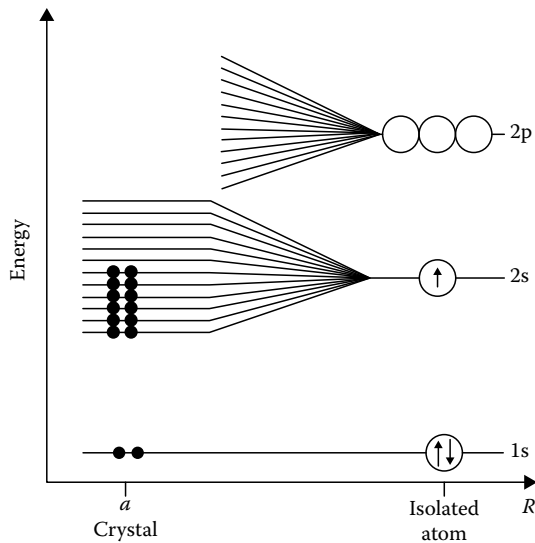


FIGURE 1.15 Band formation process for a Li crystalline solid.

The electronic states within an energy band are filled progressively by pairs of electrons in the same way that the orbitals of an atom are filled in accordance with the Pauli principle. This means that for lithium, the electronic states of the 2s band will be exactly half filled (Figure 1.15).

To summarize, the formation of a 2s-energy band from the 2s orbitals when N Li atoms are gathered together to form the Li crystal is shown in Figure 1.15. There are, N 2s-electrons but there are $2N$ states in the band, therefore the 2s band is only half full. Besides, the atomic 1s orbital, which is close to the Li nucleus, that is, is the two 1s electrons which are the core electrons, remains undisturbed in the solid, that is, each Li atom has a closed K-shell, specifically a full 1s orbital. Consequently, in general, when a solid metal is formed, the external orbitals overlap. As a consequence of this process, the outer electrons move without restraint through the metal, while the core electrons remains in their atomic orbital.

On the other hand, in covalently bonded materials like carbon, silicon, and germanium, the formation of energy bands first involves the hybridization of the outer s- and p-orbitals to form four identical orbitals, ψ_{hyb} , which form an angle of 109.5° with each other, that is, each C, Si, and Ge atom is tetrahedrally coordinated with the other C, Si, and Ge atom, respectively (Figure 1.16), resulting in a diamond-type structure.

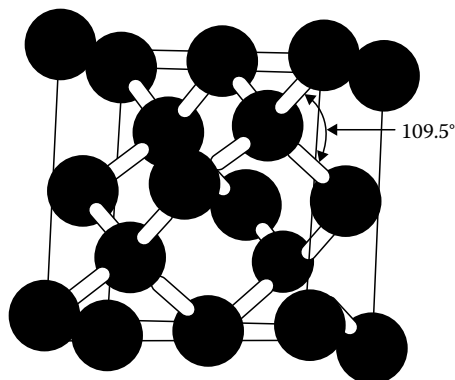


FIGURE 1.16 Tetrahedral bonding of atoms in a diamond-type structure of C, Si, and Ge crystals.

When these atoms are close enough, the ψ_{hyb} orbitals on two neighboring atoms can overlap to form a bonding orbital and an antibonding orbital [13,15]. In the crystal, the bonding orbital overlap to give the valence band, which is full of electrons, while the antibonding orbital overlap to give the conduction band, which is empty (see Figure 1.17). Since the conduction band is empty in the case of intrinsic semiconductors and insulators, these materials only conduct by the thermal excitation of electrons to the conduction band and by the formation of holes in the valence band (see Figure 1.18).

This excitation process is an activated process of electron jumps through the band gap, E_g . If the energy gap is low as in the case of semiconductors, the conductivity is low but noticeable. However, in the case of insulators, since the energy gap is high, the conductivity is very low.

Similarly, the covalent compound ZnS (zinc blende) is a semiconductor that has a structure similar to diamond, where the Zn atoms occupy the FCC lattice sites, and the S atoms occupy four of the eight tetrahedral sites of the FCC lattice (see Section 1.2.2). Analogous semiconducting properties are obtained when elements from the IIIA and VA columns of the periodic table are formed, for example, InAs, GaAs, and InP and also in the case when elements from the IIB and VIA columns of the periodic table are created, for instance, ZnTe and ZnSe.

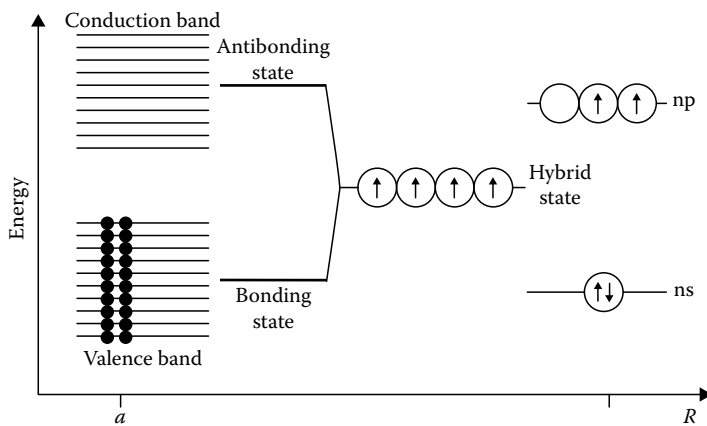


FIGURE 1.17 Band formation process for a C, Si, Ge, or α -Sn crystal.

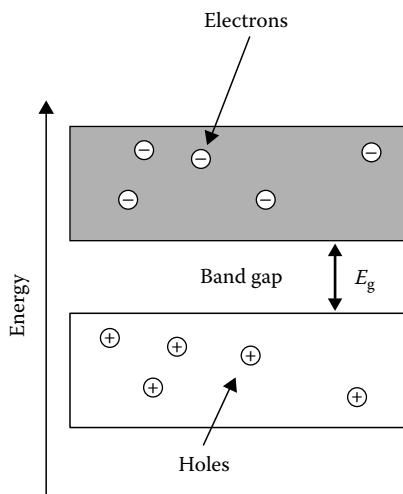


FIGURE 1.18 Formation of holes in the valence band by thermal excitation of electrons to the conduction band.

1.6 X-RAY DIFFRACTION

1.6.1 GENERAL INTRODUCTION

X-ray diffraction [20–26] is the most powerful method for the study of crystalline materials. The effect of x-ray generation during a glow discharge was casually discovered in 1895 by Wilhelm Röntgen at the University of Würzburg in Germany. Some years later, in 1912, at the University of Munich, Max von Laue and collaborators carried out one of the most important experiments of modern physics, the Laue–Knipping–Friedrich experiment, which established that x-radiation consisted of electromagnetic waves. Additionally, the experiment clearly showed that the crystals were composed of atoms arranged on a space lattice, since the electromagnetic x-ray radiation was interfering during its scattering by the crystal atoms.

To generate an x-ray beam, a vacuum tube is needed where an electron beam, produced by a heated filament, is collimated and accelerated by an electric potential of several kilovolts, that is, from 20 to 45 kV (Figure 1.19). This beam is directed to a metallic anode (Figure 1.19). The electrons hitting the anode will convey a fraction of their energy to the electrons of the target material, a process resulting in the electronic excitation of the atoms composing the metallic anode. The x-ray tube has to be evacuated to allow electron movement. Finally, in order to dissipate the heat produced by this process in the metallic anode, it is normally water cooled.

The x-ray tube produces two kinds of radiations: the continuous spectrum (Figure 1.20) and the characteristic spectrum (Figure 1.21). The continuous spectrum is a plot of the intensity of the x-ray

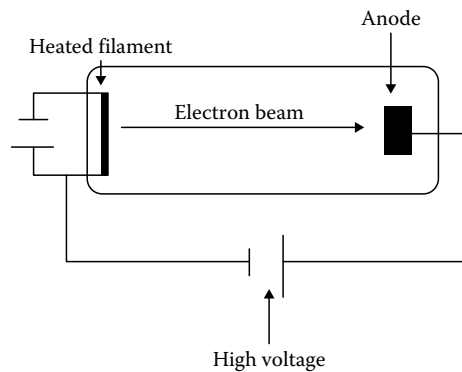


FIGURE 1.19 Schematic representation of an x-ray tube.

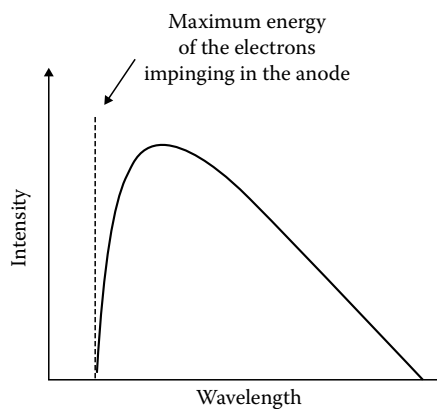


FIGURE 1.20 Schematic representation of a continuous spectrum.